SUPERCONDUCTING PROXIMITY EFFECT IN SINGLE-CRYSTAL NANOWIRES

A Dissertation

by

HAIDONG LIU

Submitted to the Office of Graduate Studies of
Texas A&M University
in partial fulfillment of the requirements for the degree of

DOCTOR OF PHILOSOPHY

May 2009

Major Subject: Materials Science & Engineering

SUPERCONDUCTING PROXIMITY EFFECT IN SINGLE-CRYSTAL NANOWIRES

A Dissertation

by

HAIDONG LIU

Submitted to the Office of Graduate Studies of
Texas A&M University
in partial fulfillment of the requirements for the degree of

DOCTOR OF PHILOSOPHY

Approved by:

Co-Chairs of Committee,	Wenhao Wu
	Joseph H. Ross Jr.
Committee Members,	Glenn Agnolet
	Haiyang Wang
Interdisciplinary Faculty Chair,	Tahir Cagin

May 2009

Major Subject: Materials Science & Engineering

ABSTRACT

Superconducting Proximity Effect in Single-Crystal Nanowires. (May 2009)

Haidong Liu, B.S., Jilin University; M.S., Nanjing University;

M.S., Texas A&M University

Co-Chairs of Advisory Committee: Dr.Wenhao Wu
Dr. Joseph H. Ross Jr.

This dissertation describes experimental studies of the superconducting proximity effect in single-crystal Pb, Sn, and Zn nanowires of lengths up to 60 μm, with both ends of the nanowires in contact with macroscopic electrodes that are either superconducting (Sn or Pb) or non-superconducting (Au). The Pb, Sn, and Zn nanowires are fabricated using a template-based electrochemical deposition method. Electric contacts to the nanowires are formed *in situ* during electrochemical growth. This method produces high transparency contacts between a pair of macroscopic electrodes and a single nanowire, circumventing the formation of oxide or other poorly conducting interface layers. Extensive analyses of the structure and the composition of the nanowire samples are presented to demonstrate that (1) the nanowires are single crystalline and (2) the nanowires are clean without any observable mixing of the materials from the electrodes.

The nanowires being investigated are significantly longer than the nanowires with which electrode-induced superconductivity was previously investigated by other groups. We have observed that in relatively short (~6 μm) Sn and Zn nanowires, robust

superconductivity is induced at the superconducting transition temperatures of the electrodes. When Sn and Pb nanowires are in contact with a pair of Au electrodes, superconductivity is suppressed completely. For nanowires of 60 μm in length, although the suppression of superconductivity by Au electrodes is only partial, the induced superconductivity at the higher transition temperatures of the electrodes remains full and robust. Therefore, an anomalous superconducting proximity effect has been observed on a length scale which far exceeds the expected length based on the existing theories of the proximity effect. The measured current-voltage characteristic of the nanowires reveals more details such as hysteresis, multiple Andreev reflection, and phase-slip centers. An interesting relation between the proximity effect and the residual-resistance-ratio of the nanowires has also been observed. Possible mechanisms for this proximity effect are discussed based on these experimental observations.

ACKNOWLEDGEMENTS

I would like to express my deep appreciation to my research advisor, Dr. Wenhao Wu, for his extensive hands-on teaching in the lab and tireless inspiration during my time as a Ph.D. student. He led me into the field of superconducting nanowires. With his insight and expertise, I have had a lot of fun solving difficult technical problems and observing many interesting phenomena. I also want to thank Dr. Joseph Ross, the co-chair of my advisory committee, Dr. Glenn Agnolet, Dr. Haiyang Wang, and Dr. Philip Hemmer, who served on my advisory committee, for their incisive observations and suggestions to my research project. Dr. Donald Naugle has always been very helpful in providing suggestions and great ideas. His generosity in allowing me to access his lab and instruments is greatly appreciated.

I want to extend my gratitude to Dr. Zuxin Ye who has been working with me everyday in the lab and helping me in various aspects of the experiments. His help in developing this project has been instrumental. During the past years, Dr. K. D. D. Rathnayaka, better known as Daya, has played an important role in every stage of my research project. Besides all the help he has provided me in fixing instruments, building new chambers, and solving other problems that I have encountered in running the experiments, he has also inspired me and taught me a great deal to become a good experimentalist and a better researcher in general. Dr. Zhiping Luo from the Microscopy and Imaging Center has also given me tremendous help in learning the necessary structural analyses through various microscopy studies. He has taught me many

techniques in operating the Transmission Electron Microscope (TEM) for investigating the structure and the composition of the nanowire samples.

I also would like to thank many of my friends and colleagues, and many among the faculty and staff in the Department of Physics, for making my time at Texas A&M University a great experience. The help from Mr. Tom Weimar and his staff in the Physics Machine Shop is extensive and essential. The support from the Electronic Shop has also been great. I want to thank Sandi Smith, who has made the life of every international student much easier in this Department. My compliments also go to Jan Gerston of the Materials Science & Engineering program, who has been a great source of information and a wonderful friend of mine.

At last, I especially want to thank my parents and other family members who have given me their unconditional support and encouragement. With their love, I can feel strong during hard times.

TABLE OF CONTENTS

Page

LIST OF FIGURES

FIGURE Page

FIGURE Page

1. INTRODUCTION: BACKGROUND AND MOTIVATION

This section gives an introduction to the field of nanowires, in particular, superconducting nanowires. Details will be provided on our method of fabricating nanowires and the properties of the nanowires we have been studying. A review of the superconducting proximity effect in nanowires will also be presented. Finally, an overview of our experimental studies will be introduced.

1.1 Nanowires fabricated by a template-based method

Nanowires are of great current interest [1, 2]. In addition to the fabrication and characterization of the nanowires and related devices [3], the unique physical properties resulting from the reduced size have been the focus of research [4].

In general, various fabrication methods can be categorized as either a top-down or a bottom-up approach. In the top-down approach, bulk materials or thin films are etched or micro-machined to form one-dimensional wires by using lithography techniques [5, 6]. This approach provides a well-controlled topography and is suitable for large scale integration [7]. The top-down approach has been widely used in the semiconductor industry.

This dissertation follows the style of Physical Review Letters.

The bottom-up approach grows nanostructures by either employing a self-assembly mechanism or using nano-sized templates [8, 9]. Self-assembly methods include the Longmuir–Blodgett (LB) process [10], the vapor-liquid-solid (VLS) method [11], and other chemical vapor deposition (CVD) methods using nano-sized catalysts [12]. The nano-template methods utilize a prepared structure to conform chemical or physical growth into a template having the desirable shape and size [2, 13]. Template-based electrochemical deposition is one of such methods. This method tends to produce materials of better quality than those produced by the top-down approach, although integration on a large scale can be challenging [14].

Nanowires fabricated by electrochemical deposition (ECD) have been studied broadly as ECD is a rather simple fabrication procedure and can produce a large variety of nanowires. By controlling the growth conditions such as the temperature, the deposition voltage, the electrolyte composition, either polycrystalline [15] or single crystalline nanowires of metals [16], alloys [17], semiconductors [18], or oxides [16] can be fabricated in ambient condition. In ECD, porous anodic aluminum oxide (AAO) or track-etched polycarbonate (PC) membranes are widely used as the templates for nanowire growth. These commercially available molecular membranes are traditionally used for filtration purposes. Nevertheless, the fabrication of AAO membranes having a well-ordered nanopore array remains a relatively active subject of research [19]. By using a standard electrochemical anodization process, AAO membranes with pores of well-controlled size and order can be fabricated [20]. Furthermore, the template-based electrochemical approach can potentially be integrated into the standard silicon

processing techniques as electroplating is already a widely used mature technique in the semiconductor industry [21, 22].

In addition to mechanical [23], electrical [24], optical [25, 26] and magnetic properties [27], superconductivity in such nanowires has been an active research subject as one-dimensional superconductors may have unique properties when their thickness is comparable to the superconducting coherence length [28-30]. For studying superconducting properties in nanowires, contrasting results have been found in granular, polycrystalline, and amorphous wires fabricated by sputtering or evaporating techniques [31-33]. This makes single-crystal nanowires an ideal candidate to study the effect of one-dimensional (1D) confinement in superconducting systems.

1.2 Superconductivity in nanowires and nanotubes

A fundamental question in superconductivity is how the collective properties of superconductors is changed when the system dimensions are reduced [34]. Within the framework of the classical theory of superconductivity, as the size of the superconductor is reduced to close to the superconducting coherence length, $\xi(T)$, the properties are expected to change radically [35-37]. When Cooper pairs are squeezed into a small volume, their wave functions are strongly modified, and therefore nanoscale superconductors are expected to exhibit properties significantly different from those of bulk superconductors. For example, when the diameter of the nanowire is comparable to or even smaller than $\xi(T)$, its behavior is expected to change from that of bulk and cross over to that of a one-dimensional (1D) or quasi-one-dimensional one [38, 39]. This

issue is also of practical importance in finding the size limit of a superconducting wire for potential applications in the integrated circuits (IC) industry [40, 41].

From the author's perspective, most works that have been reported on superconductivity in nanowires can be divided into two categories: interesting properties due to the size effect of the one-dimensional nature and the proximity effect in nanowires and nanotubes. We will introduce the proximity effect in the next subsection. In the first category, the key question to ask is whether there is a size-limit for a sample to conduct supercurrents? And if there is, what is the limit? Qualitatively, for a long 1D channel in the case of a quantum wire, since there is only one channel for supercurrent to flow, there is always a finite probability that thermal fluctuations may drive a fraction of a wire into normal. Theoretical predictions as well as recent experimental studies have shown that below a certain size limit, a superconductor nanowire acquires a finite resistance due to quantum fluctuations [42-44]. The fluctuations can destroy the superconducting state even at temperatures close to zero.

In a well-known work by Bezryadin *et al.* [34], an insulating state was observed for nanowires with normal state resistance larger than the quantum resistance for Cooper pairs, $h/4e^2$. Such nanowires with diameters smaller than 10 nm were produced by coating carbon nanotubes with MoGe alloy. The authors attributed the suppression of superconductivity to quantum phase slips along the wires. In another work by Zgriski *et al.* [45], breakdown of superconductivity was also found experimentally in ultrathin (~10 nm) and homogeneous aluminum nanowires. The authors also observed an evolution of

the shape of $R(T)$ and the critical temperature value as a function of the effective diameter.

Another intriguing effect is, as reported by Rogachev *et al.* [46], a critical current enhancement by a magnetic field at low temperatures in ultra narrow, sub-10-nm MoGe and Nb superconducting wires. This effect was found to be stronger for narrower wires. The authors conjectured that local magnetic moments generated by surface oxides could quench the exchange coupling between external fields with the electrons in Cooper pairs, thereby, enhancing the critical current. In a recent work by Tian *et al.* [47], an anomalous anti-proximity effect (APE) was observed in Zn nanowires of 40 nm in diameter. Superconductivity in the Zn NWs is suppressed either completely or partially by superconducting electrodes. When the electrodes are driven into their normal state by a magnetic field, the nanowires switch back to their superconducting state. This effect is not seen in wires of diameters 70 nm or larger. This anti-proximity effect is not well understood.

The development of a finite resistance and the suppression of superconductivity below T_c in nanowires have typically been explained in terms of phase-slip-centers (PSC), which was initially proposed by Skocpol, Beasley, and Tinkham (SBT) [48]. PSC refers to segments along a superconducting nanowire or filament, where the superconducting order parameter fluctuates about zero [37]. Across the segment, the phase of the superconducting order parameter slips by 2π. This phase slip results in a voltage across the segment and the nanowire becomes resistive. The concept of PSC was first proposed to explain the regular steps in the *I-V* curves of tin whiskers [48] and

superconducting microbridges [49]. Although this behavior was first observed in conventional superconductors, it is also present in high-temperature superconductors [50, 51]. In a recent paper, phase slips was explained as the dual process to Cooper-pair tunneling in a Josephson junction [43]. Although phase slips by thermal activation at high temperatures are well accepted and understood, the existence of quantum-phase-slips (QPS) at low temperatures is still under debate [42]. The simplest geometry to study PSCs is a 1D superconductor with a diameter smaller than the coherence length.

1.3 Superconducting proximity effect in one dimension systems

The proximity effect (PE) at a superconductor (S) and normal-metal (N) interface is a well known effect [37]. Early studies were focused on the modulation of the critical temperature T_c in layered S-N systems. When a normal metal N is deposited on top of a superconductor S, and if the electrical contact between the two is good, Cooper pairs can leak from S to N. A review of early studies of the proximity effect was done by Deutscher and De Gennes in 1969 [36].

Recent experiments have drawn interest to the proximity effect in micro-scale and nano-scale systems in which cases electrical transport can be greatly affected by the presence of macroscopic superconducting or normal leads. Many interesting and sometimes surprising results have been reported. As early as in the beginning of 1990's, Courtois *et al.* [52] found that a narrow metallic (Cu or Ag) wire of length up to 1.6 μm can have zero resistance when they were connected to superconducting Al islands. Low temperature results measured in such systems turned out to diverge significantly from

the classical models in both the clean limit and the dirty limit. In another work around the same time, using lithographically defined aluminum microstructures, Kwong *et al.* [6] observed a substantially more robust proximity effect over a surprisingly long range (50 μm) which was inconsistent with theoretical models. The authors commented that quasi-particle coherence might play an important role in the results.

With the current nanofabrication techniques, new results have been obtained in structures with even smaller sizes, especially, semiconductor nanowires and carbon nanotubes. In a report by van Dam *et al.* [53], n-type InAs nanowires (NWs) were interconnected by aluminum pads to form a superconducting quantum interference device (SQUID). Supercurrents were found to flow through the quantum-dot-like weak link formed by a semiconductor-superconductor junction. Interestingly, they also demonstrated that, by adding a single electron with certain spin configuration to the quantum dot using a gate electrode, the supercurrent can reverse its sign. In another work by the same group [54], a prototype of quantum supercurrent transistor is realized by defining aluminum electrodes on a carbon nanotube. Also in one of the earliest works to report proximity-induced superconductivity in single-walled carbon nanotubes, Kasumov *et al.* [55] emphasized the importance of obtaining highly transparent contacts between the superconducting electrodes and the carbon nanotubes.

The proximity effect is intimately related to the Andreev reflection of electrons at the N-S interface [56], where many intriguing properties have been measured. Andreev reflection is a microscopic mechanism of the proximity effect, in which one electron coming from N is reflected as a coherent hole, while a Cooper pair is transmitted into S.

One popular and successful model to describe the Andreev reflection at an S-N interface is established in a 1982 paper by Blonder, Tinkam and Klapwijk (BTK) [57]. In this paper, a ballistic Andreev reflection model was proposed and a simple theory for simulating *I-V* curves of an S-N micro-constriction was presented. According to this model, Andreev reflection takes place in S over a distance equal to the superconducting coherence length. In this picture, coherence is lost in the normal metal at a certain distance from the interface, which should be smaller than the coherence length in the normal metal L_ϕ and the thermal length L_T which is $2\pi\hbar v_F/k_BT$ in the clean limit and $\sqrt{(\hbar D/k_BT)}$ in the dirty limit [58], where ħ is Planck's constant, k_B is the Boltzmann constant, v_F is the Fermi velocity, and D is the electron diffusivity. At a few degrees Kelvin, L_T is no more than a few microns for typical metals and is larger than L_ϕ. In the clean limit, L_T is 2 μm at 7.2 K and 3.8 μm at 3.7 K for Sn and Zn. This picture is consistent with reports on the PE in carbon nanotubes, semiconductor nanowires, and graphene of length 0.1-0.5 μm, as well as e-beam patterned Al NWs [59] and electroplated Sn NWs of length up to 4 μm [60]. However, exceptions exist. In addition to a modulation of T_c on a length scale of 60 μm observed earlier by Kwong *et al*. in lithographically patterned Al films, we have observed an anomalous PE in single crystalline Zn, Sn, and Pb NWs of length up to 60 μm, which can not be explained by existing theories [61]. More details about this anomalous long-range proximity effect will be presented in this dissertation.

1.4 Design of experiments

Many efforts have been made to make our study of the superconducting proximity effect in nanowires unique and effective. When defining an electrode-nanowire-electrode structure, our *in situ* electrodeposition method directly grows nanowires on one electrode and connects to the other electrode as the deposition process is completed. By choosing different materials (normal or superconducting) for the electrodes and nanowires, we can study both the suppression and induction of superconductivity in the nanowires. The length of the nanowires was determined by the thickness of the molecular membranes. Commercially available membranes have two choices for the thickness: 60 μm for AAO membranes and 6 μm for PC membranes. These two choices give a good representation of the proximity effect in a broad range. This is because 6 μm is the upper-limit for the conventional proximity effect that has been observed while 60 μm is far beyond the length scale of the proximity effect expected by existing theories. Although we can not continuously change the diameter of the nanowires, six different sizes range from 40 nm to 200 nm provide a broad diameter range to investigate the effect of the diameter on the observed proximity effect.

Special attention was given to two issues while designing the experiments: the quality of the nanowire and the transparency of the nanowire-electrode contact. By using the electro-deposition method, we can control the growth conditions to make single-crystal nanowires. This is practically the best quality we can expect for studying superconductivity. Although we still can not exclude the effects due to the not-so-uniform diameters along the wire, the scattering due to grain boundaries and other

artifacts in polycrystalline and amorphous samples are absent. For the nanowire-electrode contact, the self-contacting technique invented by our group is believed to give a nearly perfect transparency [38, 62]. This is mainly because the connection was made in a one-step process during electroplating, thus minimizes the possibility of developing an oxide layer which often happens when a two-step process is used.

As expected, our structure achieved the desired qualities that we proposed, as reflected by both microscopic studies and transport measurements. Although the anomalous long-range proximity effect is still unexpected, we have found clues to further understand the phenomenon. Analysis from our electron transport data also suggests connections to other reported results and the current theoretical picture.

2. EXPERIMENTAL: FABRICATION AND CHARACTERIZATION OF ELECTRODE-NANOWIRE STRUCTURES

In this section, experimental methods and details will be reviewed for the fabrication and microscopy characterization of the electrode-nanowire-electrode structure. Starting with the electrodeposition methods, we describe the details of each step by focusing on the uniqueness of our experimental set-up, the *in situ* self-contacting method. Then microscopy studies using the scanning electron microscope (SEM) and the transmission electron microscope (TEM) will be presented. Since the observed long-range proximity effect is unexpected, special and advanced microscopy methods were used to specifically address the issues associated with the structure and the chemical composition of the samples. In particular, in addition to imaging extracted nanowires after the membranes have been dissolved as is often done in most works [29, 63], we have developed several methods to investigate the structure and the composition of the nanowires still remaining in their original membrane pore channels, and, in some cases, still in contact with the bulk film electrodes.

2.1 Nanowire fabrication using electro-deposition

The nanowires were fabricated using a template-based electrochemical approach which has been reported by an increasing number of groups for producing a great variety of NWs [32, 33, 64, 65]. This method is essentially an electroplating technique utilizing

the nanometer sized pore channels in molecular membranes as templates. Anodic aluminum oxide (AAO) and track etched polycarbonate (PC) membranes are the most widely used porous membranes. They are commercially available due for application as filters in biological processes. Most membranes used in our experiments are purchased from commercial venders. We can also fabricated AAO membranes with a much better honeycomb pore order. A top view and a cross-section view of home-made membranes are presented in Fig. 2.1. From the side view, we confirm that the nano-channels are uniform along the length. Such membranes are fabricated by anodizing aluminum sheet in acid solutions. It is well established that, by controlling parameters such as voltage and pH value, etc, the pore size and the thickness of the membrane can be finely tuned [2, 66, 67]. This makes AAO membranes suitable templates for electroplating nanowires with different diameter and length.

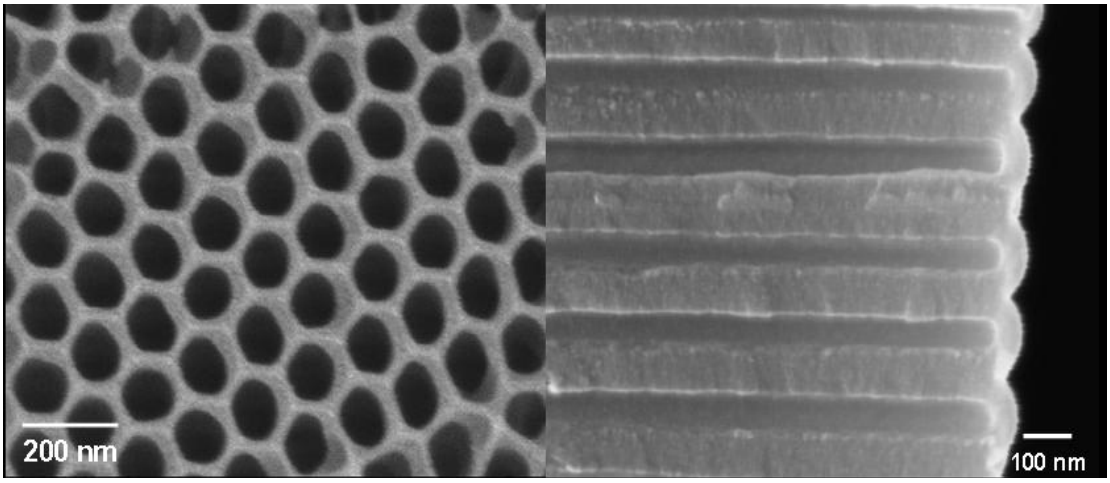

FIG. 2.1. SEM image of home-made anodic aluminum oxide (AAO) membranes. Top view (left) and side view (right)

Polycarbonate membranes are organic membranes with much better flexibility and ease in handling, compared to the hard and brittle AAO membranes. They are made by exposing thin polycarbonate sheets in well aligned particle beams. The track of a particle leaves a single channel in the PC film. An example of such membrane is shown in Fig. 2.2. The pore size in this membrane is 50 nm. Compared to the hexagonal lattice structure for AAO pores, pores in PC are randomly distributed with a pore density smaller by an order of magnitude compared to that of AAO membranes.

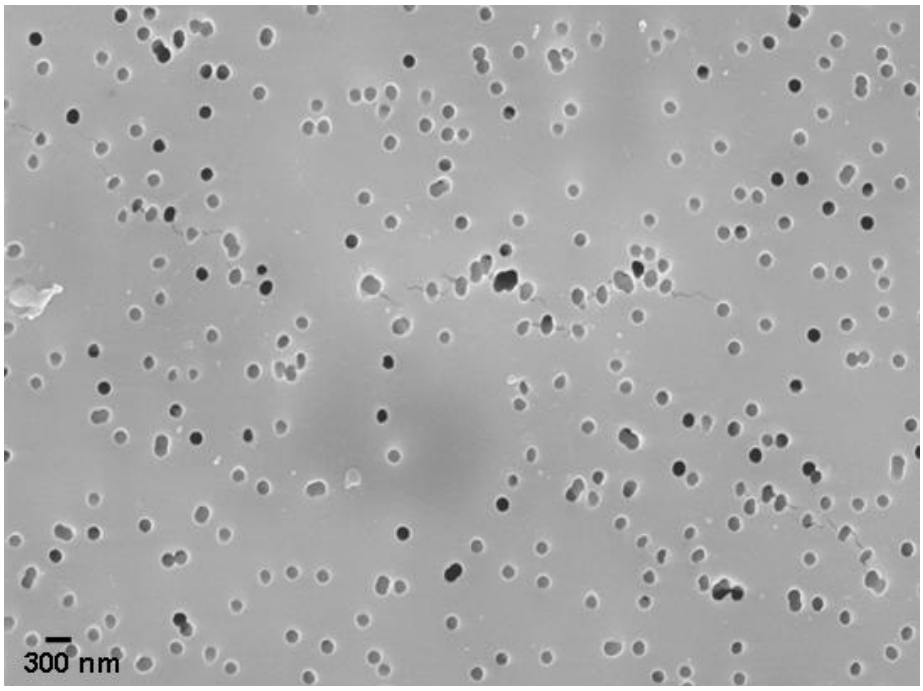

FIG. 2.2. SEM image of the top view of a track-etched polycarbonate PC membrane

We plated Pb, Sn, and Zn NWs into either thinner (6 μm) polycarbonate (PC) membranes with random pore sites or thicker (60 μm) anodic aluminum oxide (AAO)

membranes with a honeycomb pore arrangement, producing NWs of length 6 μm or 60 μm and diameters 30-200 nm or 100-250 nm, respectively. The membranes were purchased from Whatman Co. and SPI Supplies Inc.

For plating Pb, the electrolyte was a 200 ml solution with 16.2 g $Pb(BF_4)_2$ 50% wt solution in water, 6.72 g HBF_4, and 3.0 g HBO_3. For plating Sn, the electrolyte was prepared by mixing 16.72 g of a $Sn(BF_4)_2$ solution at 50 wt% with 200 ml of water. For plating Zn, the electrolyte was prepared by dissolving 4.7 g $ZnCl_2$ into 200 ml water. A Pt anode was used and the reducing potentials relative to an Ag/AgCl reference electrode were 0.4 - 0.5 V for Pb, 0.4 - 0.5 V for Sn, and 1.1 - 1.2 V for Zn. In our approach, a thick (~300 nm) Au, Sn, or Pb back electrode was evaporated on one surface of a porous membrane. It blocked all the pores to form the cathode for electroplating. The anode was placed facing the other surface of the membrane. Electroplating was initiated at the cathode and the pores were filled to form an organized field of NWs.

2.2 Contacting nanowires with electrodes: the *in situ* method

While different methods have been applied to form electric contacts on NWs for transport studies, the most reliable method is an *in situ* method which allows for contacting a single NW with a virtually zero contact resistance [38, 62]. We used one variance of this *in situ* method for the present study, as illustrated by Fig. 2.3. In addition to the thick back electrode which blocked all the pores, a relatively thinner (50-100 nm) front electrode of Au, Sn, or Pb was evaporated on the other surface of the membrane. It

blocked many of the pores and left some pores open for electroplating. A SEM image of a membrane with a 70 nm-thick Au front electrode is presented in Fig. 2.4.

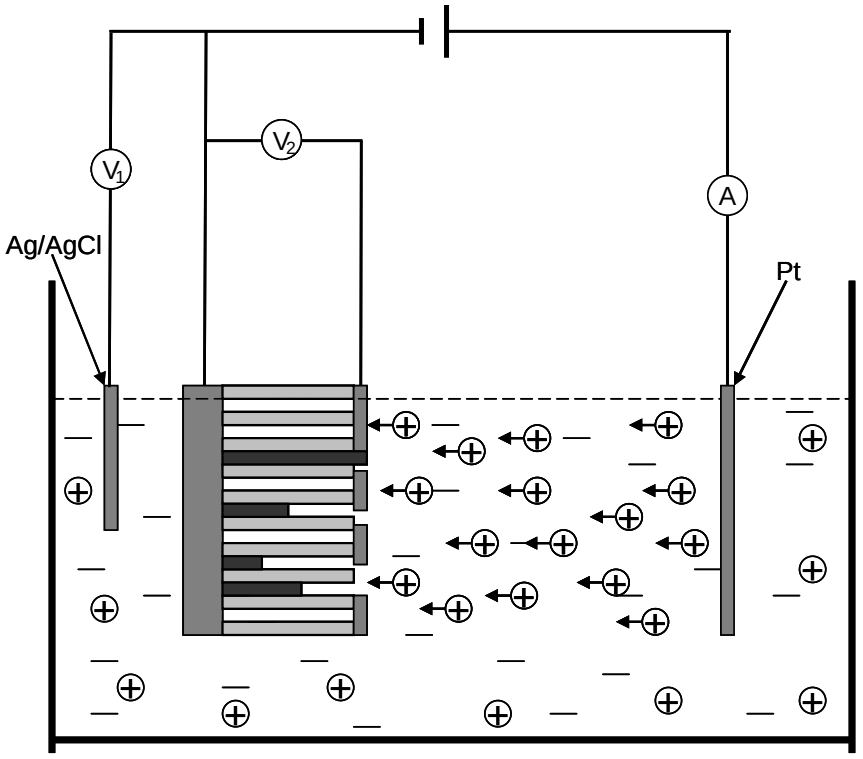

FIG. 2.3. Illustration of an electrochemical cell. Schematic of the self-contacting method can be achieved using this set-up by measuring the working potential, votage and current as V_1, V_2 and A respectively

As Fig. 2.3 shows, a voltmeter, V_1, was connected between the back electrode and the reference electrode, Ag/AgCl. To reduce one particular type of ion, a specific voltage is applied at the back electrode. This value was calculated from the concentration of ions,

temperature of the solution, pH value, and the standard electro-chemical potential of the ion.

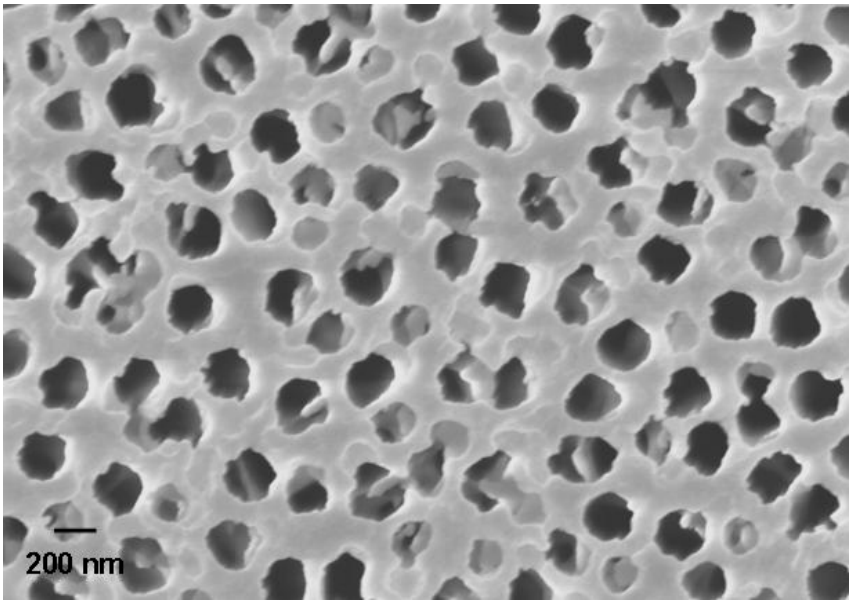

FIG. 2.4. SEM image of an AAO membrane with front electrode. A 70nm-thick layer of Au evaporated on the top of the membrane to form the front electrode. The size of the pores is around 200nm

We used a voltmeter to monitor the potential difference V_2 between the front and the back electrodes. Initially, V_2 decreased gradually as the open pores were being filled. When the fastest growing NW made a contact with the front electrode, a sudden drop in V_2 could be observed. Fig. 2.5 showed a typical example. The typical time for making such a contact varies from sample to sample, depends on the currents flowing through the circuit. The current was determined by properly set the output of the power supply, which was tuned to maintain a desirable voltage V_1. The current can be recorded during electroplating, as shown in Fig. 2.3. A jump in current was observed when a nanowire

made a connection with the front electrode. It was obvious that nanowires in different pores grow at different rates [62], as was supported by our structure characterizations shown later. Thus, there will always be some wires grow out of the membrane first and reach the front electrode

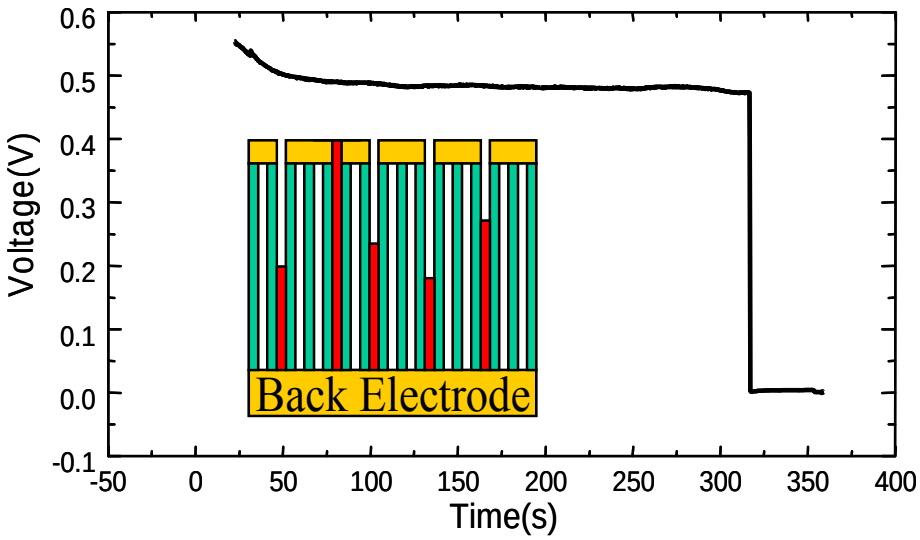

FIG. 2.5. Voltage measured between the front and back electrode during an electro-plating process. The inset graph is a schematic where a nanowire has been contacted to the front electrode

If electroplating was terminated when V_2 dropped to zero suddenly, we could obtain a sample having a single NW whose ends were in contact with the back and the front electrodes. Since such a nanowire is already connected with bulk leads, electron transport measurements can be carried out right away. In the experiments, we found that such contacts were very sensitive to the temperature, pressure change, and mechanical

vibrations. To enhance the chance of successful transport measurement, only those samples with relative stable resistance values were measured at low temperatures.

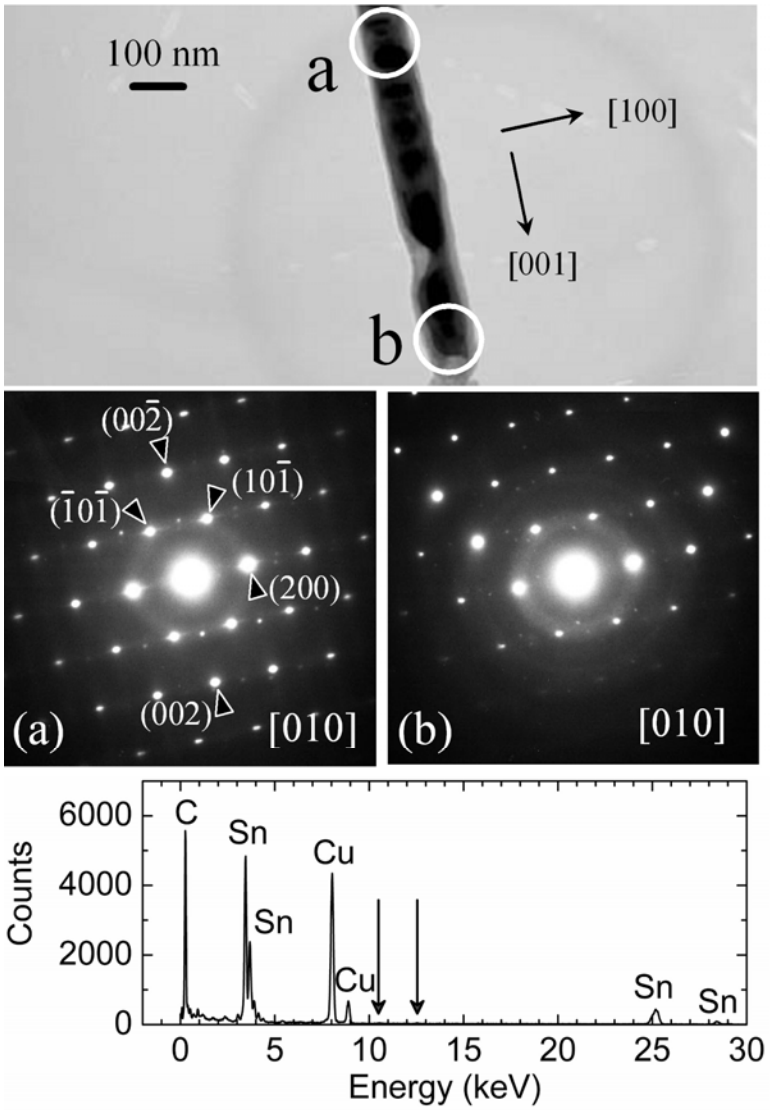

FIG. 2.6. TEM study of Sn nanowires. Top: TEM image of a Sn NW grown using Pb electrodes. Middle: EDPs taken at spots a and b in the top frame. The diffuse rings are likely from a supporting amorphous carbon film. Bottom: EDS taken on the Sn NW. C and Cu peaks are from the carbon film supported Cu grid. Pb signals, at energies indicated by two arrows, are absent

2.3 Structure and composition analysis of nanowires

In the standard approach, nanowires are extracted by dissolving the membrane (in a 4 M NaOH solution for AAO membranes and in dichloromethane for PC membranes) after polishing off the back and the front electrodes. Free standing nanowires in ethanol or water can be obtained by using a centrifuge. SEM or TEM specimen can be made by dropping the solution onto a substrate or a Cu grid.

In Fig. 2.6, we illustrate the results of a TEM study of a typical Sn nanowire grown with Pb front and back electrodes. Selected Area Electron Diffraction (SAED) patterns taken on different spots along the wire give the same pattern, indicating its single crystalline nature. Plane indexes and growth direction have been marked on the SAED pattern. The Sn nanowires have a tetragonal lattice structure, same as its bulk phase. Furthermore, the energy dispersive spectroscopy (EDS) results shown in the bottom frame in Fig. 2.6 confirms the chemical composition of the Sn nanowires, and that mixing of materials from the Pb electrode is absent.

Fig. 2.7 gives another example of a TEM study of Zn nanowire grown with Pb front and back electrodes. The wire is typical of many wires we have studied as shown in the bottom left frame. SAED patterns taken on different spots along the wire gives identical patterns as shown in the top right frame indicating its single crystalline nature. Plane indexes and growth direction have been marked on the SAED pattern. Analyses have found that the Zn nanowires have the hexagonal structure, same as its bulk phase.

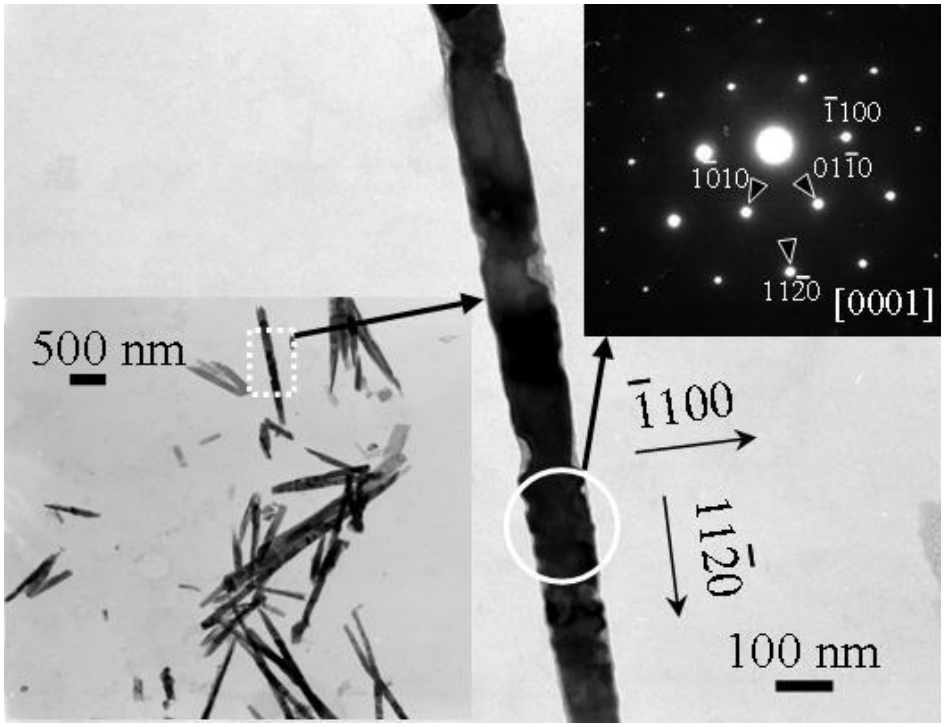

FIG. 2.7. TEM study of Zn nanowires. TEM images of free standing Zn nanowires and SAED patterns taken on the wire with plane indexes and growth direction indicated

2.4 Advanced characterization of nanowire/electrode devices

Besides identifying the composition and crystal structure of the grown wires, as we did in the last subsection, a great deal of effort has been made to investigate the interface between the nanowires and the electrode in contact with them. Due to the unexpected transport results from our measurements, such effort was necessary in order to verify the structure and the composition of the NW samples. We will present advanced microscopic structural studies based on a number of sample fabrication methods.

In the first approach, both surfaces of a membrane filled with nanowires were polished to remove the front and back electrodes and then imaged using SEM. As shown in Fig. 2.8, Zn nanowires grown in AAO membrane using Pb electrodes appear as white spots. Black spots are unfilled pores. EDS on many different spots have found no trace of mixing of Pb from the electrode. Au and Pd peaks found in the EDS spectrum are from the coating to enhance surface conductivity for SEM imaging.

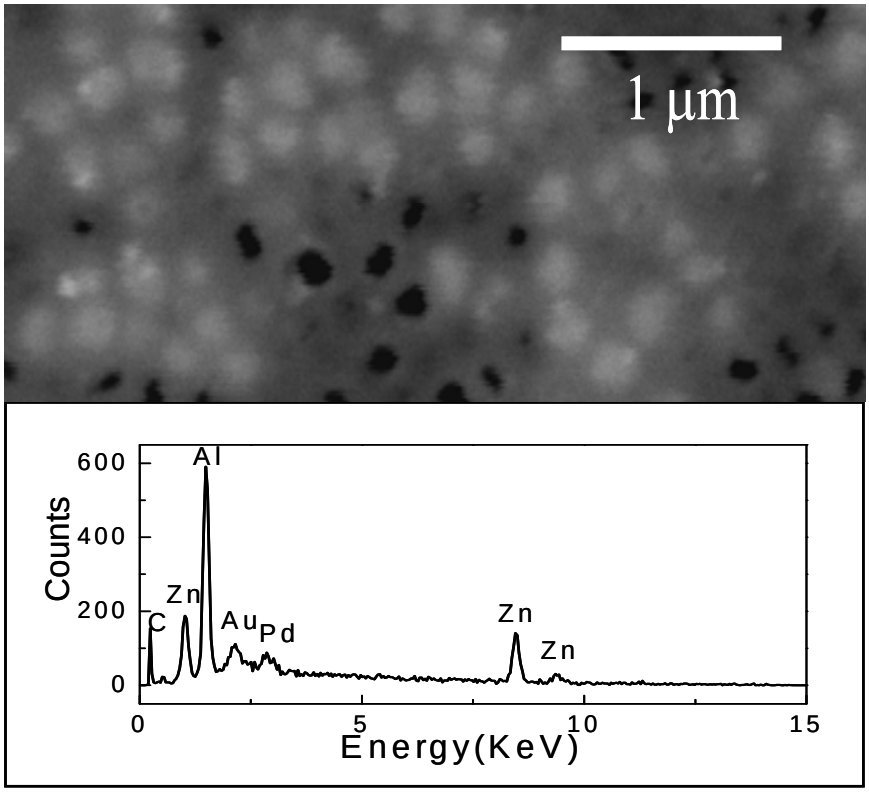

FIG. 2.8. SEM image of Zn nanowires grown in AAO membrane after Pb electrodes are polished off. EDS on the bottom shows a typical scan indicating no Pb trace found

The second approach is illustrated in the top of Fig. 2.9, in which an Ar+ ion beams are used to mill a hole through a membrane filled with nanowires after the front and back electrodes are removed. The milling angle was chosen as 15° so that the thin edge around the hole can be large enough to be viewed by TEM. Specimen made this way can provide structural and compositional information while the NWs are still preserved in the membrane. Compositional analyses over large areas and at different depths in the samples are possible if we choose the right milling angle and rate.

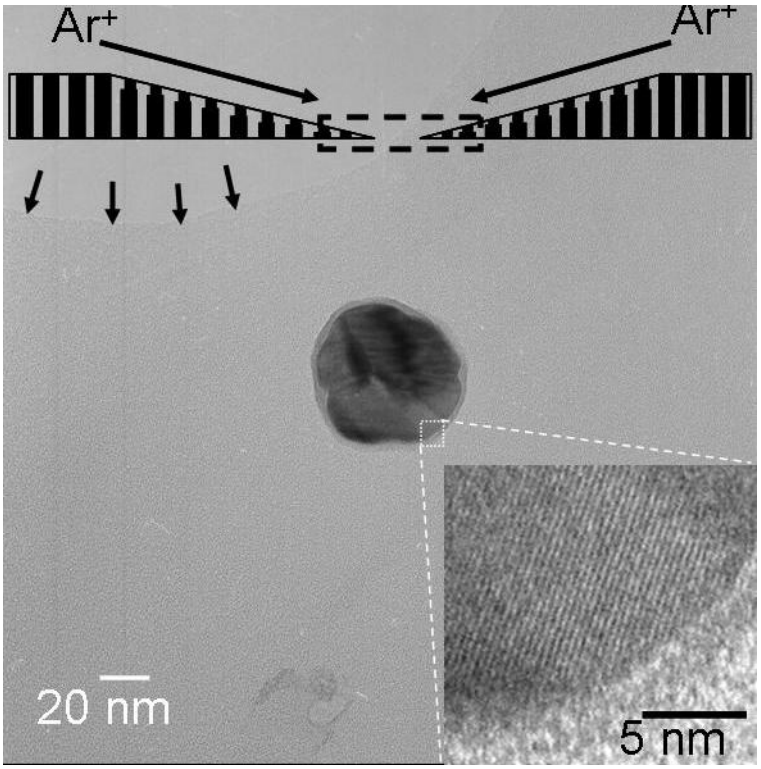

FIG. 2.9. TEM image of a cross-section of Sn nanowire in polycarbonate matrix. The image was taken after ion milling process as illustrated on the top. Arrows show the edge of an ion milled hole. Inset is the high magnification image shows the surface oxidation layer and lattice fringes

As an example, Fig. 2.9 shows the results of a TEM study of a PC membrane filled with Sn nanowires grown with Pb front and back electrodes. Black arrows indicate the edge of the milled hole. The cross-section image of the Sn nanowire indicates the actual nanowire diameter is about 60 nm while the nominal pore diameter of the PC membrane is 50 mnm. An oxidation layer around the nanowire is visible. The magnified image of the selected area at the bottom right shows the lattice fringes.

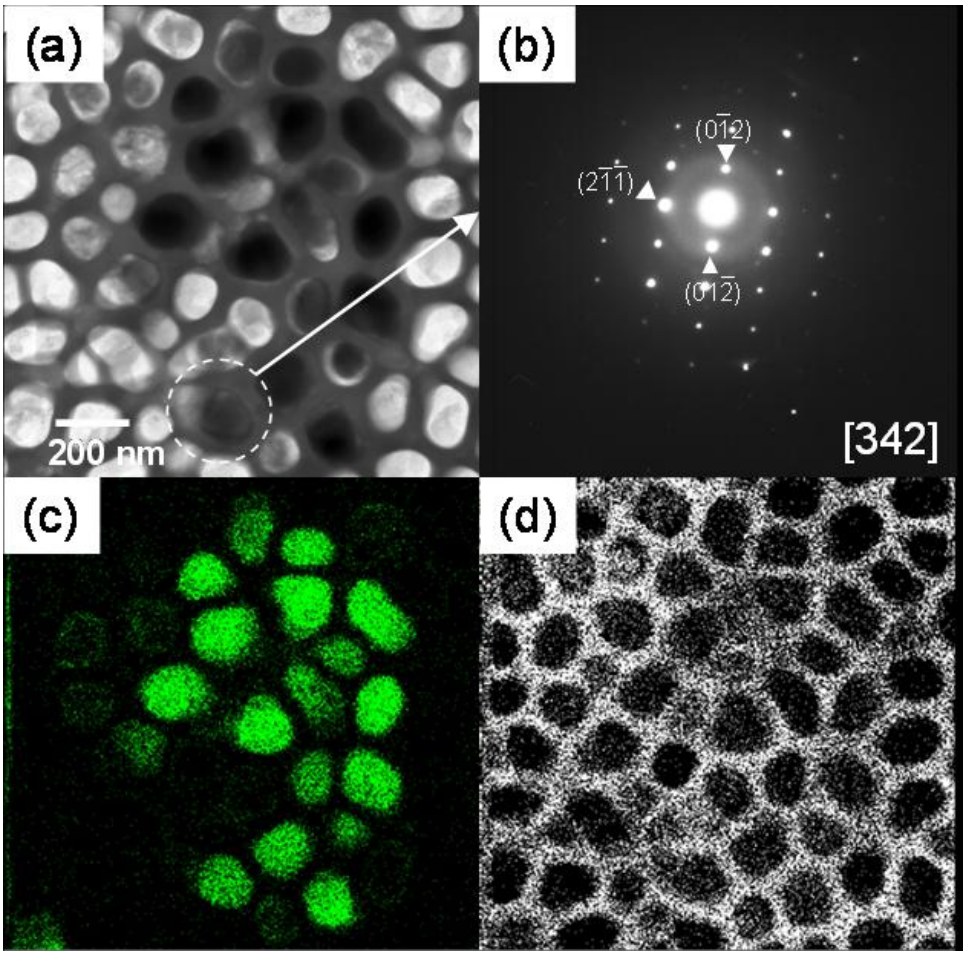

FIG. 2.10. Cross-sectional TEM study of Zn nanowires in AAO membrane. (a) TEM image of AAO membrane with Zn nanowires grown inside after Pb electrodes polished off and ion milling. (b) SAED pattern of a typical cross-section of Zn nanowires. (c) and (d) are EDS maps of the same area with element mapping of Zn and Al, respectively

Specimen made using this method can also be used for EDS mapping where compositional information can be obtained for a relatively large area. Fig. 2.10 shows such a study on a Zn NW sample grown in AAO membrane using Pb electrodes. The

TEM image in Fig. 2.10 (a) shows Zn nanowires grown in AAO membranes as black spots where SAED patterns can be taken as shown in (b). EDS maps of Zn (c) and Al (c) elements in the same area clearly identifies each Zn NW cross-section and each pore in the AAO membrane. Mapping of Pb in the area did not give any signal above the background noise level.

The third approach enables us to exam the electrode-nanowire interface while the nanowires are still preserved in their original pore channels in the template. AAO or PC membranes filled with nanowires are embedded in epoxy and cut into thin slices (< 200 nm) along the direction of the NWs using ultramicrotomy. Many thin slices can then be transferred onto carbon coated Cu grids for TEM studies. A thin layer of carbon was always evaporated onto the specimen for stabilization purpose.

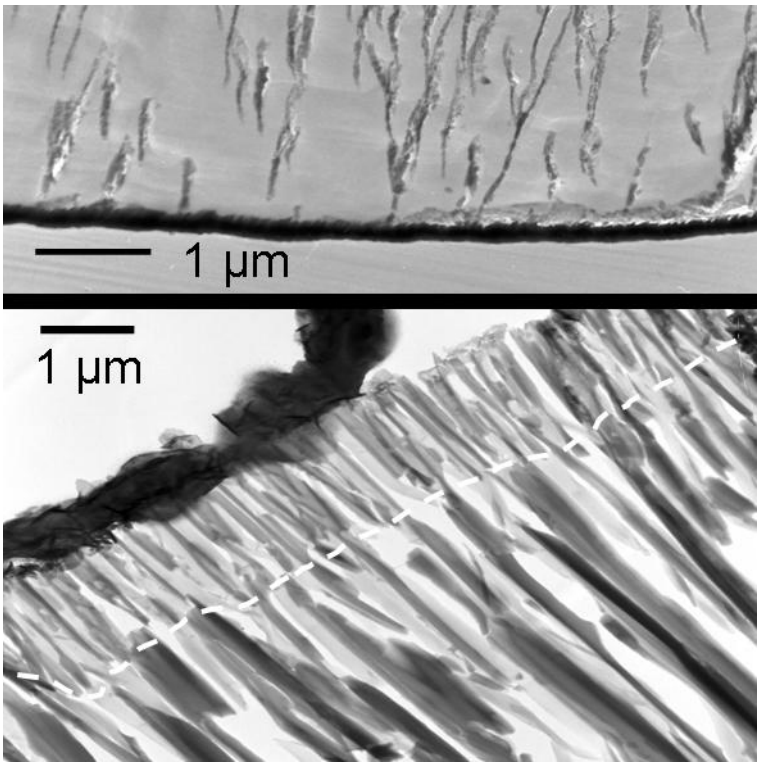

FIG. 2.11. TEM study of the electrode-membrane interface. Top: TEM image of the interface between Au electrode and polycarbonate membrane with Sn nanowires grown inside; Bottom: TEM image of the interface between Pb electrode and the AAO membrane with Pb nanowires grown inside. White lines indicated the boundary of two-layer AAO substructure

Fig. 2.11 shows Sn NWs in a PC membrane with the Au electrode appearing as the dark stripe at the edge. EDS mapping similar to that in Fig. 2.12 didn't find any Au trace inside the membrane. This is consistent with a clean Au-PC interface. Another sample with Zn nanowires grown in AAO membrane with Pb electrode is shown at the bottom of Fig. 2.11. Besides showing a clean Pb-AAO interface, this image also shows that commercial membranes from Whatman have a two-layered structure, as was suggested

by many groups [16, 67]. It is clearly shown in Fig. 2.11 that in a surface layer with a thickness of about 1 μm the pore diameter is about half as large as the pore diameter in the bulk of the membrane. To our knowledge, this image is the first one to directly show such a two-layered structure details of the AAO membranes. A clear indication of layer interface was shown by the white dashed line in the figure. We have not been successful in observing a similar feature in the PC membranes, although a similar structure was suggested [16] for PC membranes.

The main purpose of our microscopy study is to investigate the device structure in detail to obtain a clear picture of where nanowires are grown and how electrode materials distribute. This method offers an efficient way to further investigate details of compositional distribution across the sample. By employing the same method of EDS mapping, we can obtain compositional information along the length of each nanowire, where an area with many nanowires can be studied in one scan. Such a study on a Pb/ZnNW/Pb sample made with AAO membrane is shown in Fig. 2.12. In the TEM image, dark areas are nanowires embedding in AAO membranes. In principle, we can carry out EDS scans on any part of the area from the top electrode to the bottom electrode to map out the distribution of Al, Zn, and Pb elements. Based on all the studies we have done, no signal for the electrode material has been found in the nanowires.

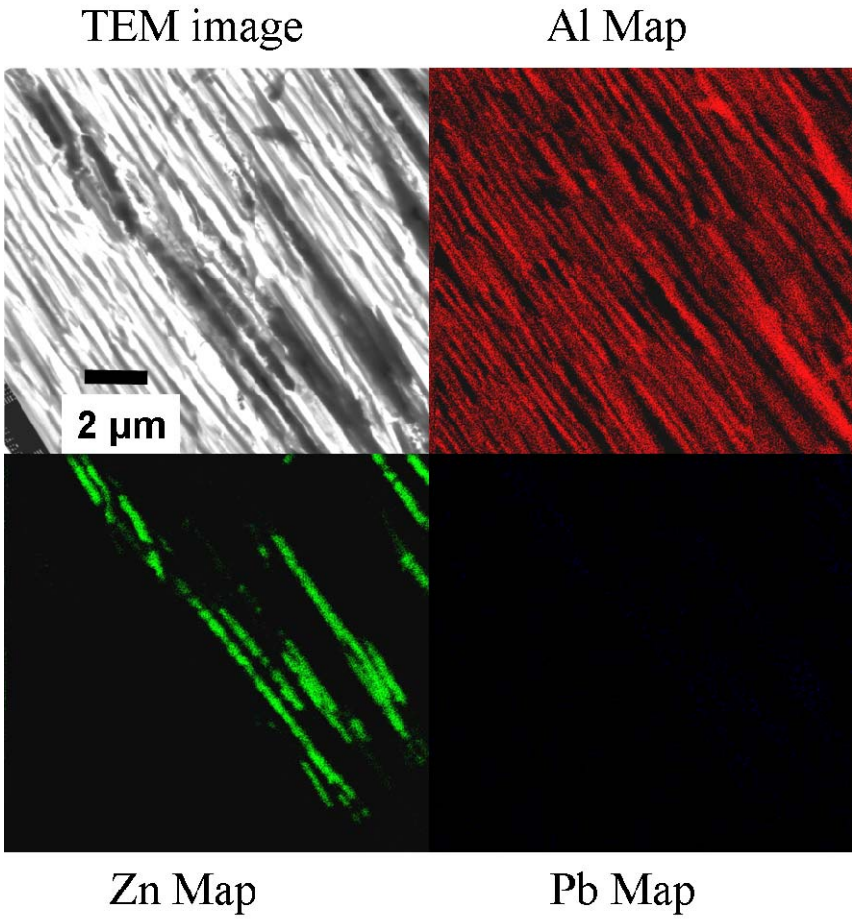

FIG. 2.12. Compositional study of a long Pb/ZnNW/Pb sample with NWs remaining in AAO membranes. With the TEM image showing the actual area we are stuying, the EDS mapping gives elemental signal distribution across the area as indicated

The information obtained in Fig. 2.12 shows that there is not mixing of electrode materials inside the membrane. However, it will be better if we can image the electrode material and the nanowires which are in contact with them at the same time. We have tried many specimens and success was finally achieved in the sample shown in Fig. 2.13.

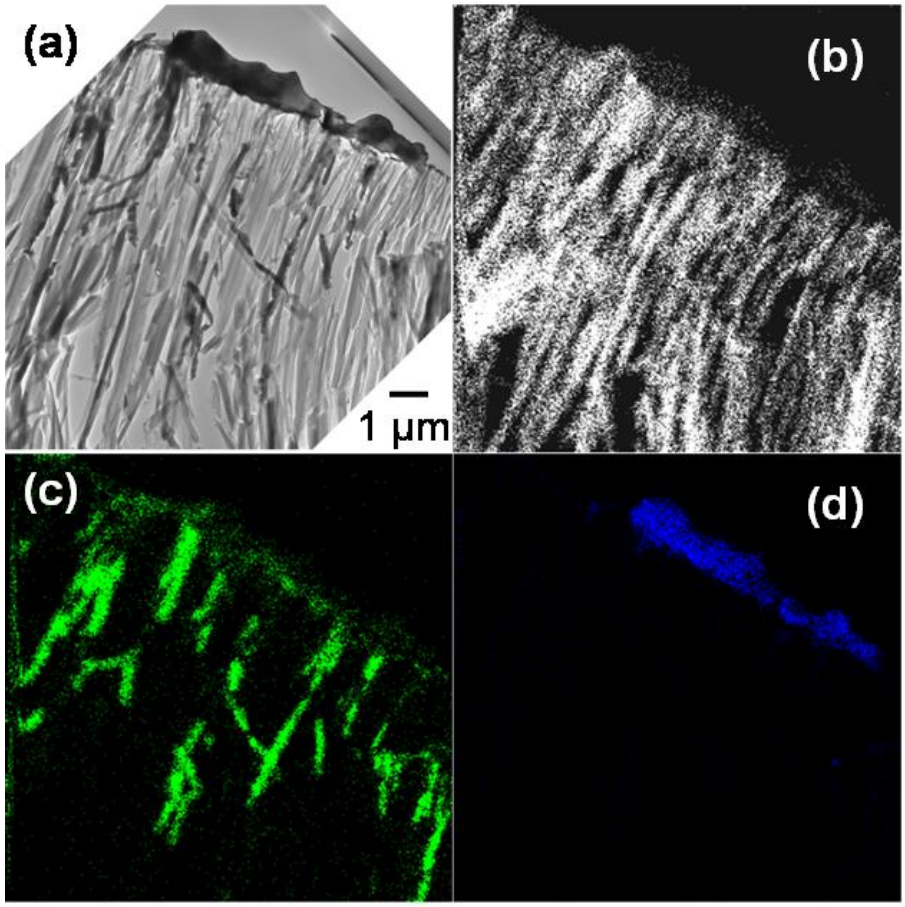

FIG. 2.13. TEM study of Pb electrode-Zn NWs interface. (a) TEM image of the side view of Zn NW grown between Pb electrodes in AAO membrane. (b-d) EDS maps of the same area with element mapping of Al, Zn and Pb, respectively; Each element was represented by one specific color

In Fig. 2.13, a Pb/ZnNW/Pb sample in AAO membrane is imaged while the electrode is found to be in contact with many nanowires. To confirm the chemical composition of the NWs, EDS studies were done on such specimens. Fig.2.13 (b-d) shows the EDS maps for elemental Al, Zn, and Pb, respectively. Fig.2.13 (a) shows the TEM image of the same area where both Zn NWs (black stripes) and Pb electrodes (grey

block on the top) can be seen. Again, we demonstrate that the Zn NWs were grown inside the membrane with no mixing of the electrode material. This study, along with many other similar studies, also supports the fact that nanowires grow at noticeably different rates in electrodeposition.

Based on all the analyses and observations, we can exclude the possibility of diffusion of the electrode material into nanowires for the following reasons: (1) typical observations and measurements for fabricated devices indicate that there are wires grown between the front and back electrodes with a resistance similar to that of the nanowires we intend to grow and they will grow into single crystals made of the same material as nanowires that we intended to grow; (2) it is chemically unfavorable for the electrode material to dissolve in the plating process and be reduced to its metallic form under the same condition where the working potential was adjusted to reduce another kind of cations of a higher reactivity; (3) there is no observable change to the front and the back electrode during electroplating, further confirming that the electrodes are not reactive to the solution; (4) Detailed structural studies indicate that the electrodes remain intact after ECD and no diffusion of electrode material into the membranes were found; (5) Detailed structural studies also prove that many nanowires were actually grown into the membrane as we expected and no nanowire made of the electrode material was found; (6) Transport measurement on over 160 samples didn't yield any exceptions.

We note that the four types of SEM and TEM studies described above do not directly image the particular single nanowires that were contacted for transport measurements.

However, based on the principle of electroplating, there is absolutely no reason for these single nanowires used for transport measurements to be different from those imaged in SEM and TEM studies. Our SEM and TEM studies, which together form the most comprehensive SEM and TEM studies have so far been performed on template-grown nanowires systems, have shown clearly the structure and the composition of the nanowires. In particular, they have demonstrated convincingly that there is no mixing of the materials from the front and back electrodes into the nanowires. Therefore, we conclude that we have observed an anomalous long-range superconducting proximity effect in single crystal nanowires.

2.5 Low temperature transport measurements

The low-temperature electrical resistance measurements of the electrode-NW-electrode devices were done immediately after the fabrication process. In the schematic in Fig. 2.3, a small piece of membrane (usually in the size of 4 mm x 5 mm) is mounted on a surf board (with dimension of 8 mm x 14 mm). The board has three build-in leads with platinum coating on top of Cu pads. The middle lead is usually put in contact with the back electrode on one side of the membrane using silver paint or soft solder. Each of the other two leads is connected with a corner of the front electrode. Such configuration allows us to measure the resistance between the front and back electrode, i.e. the nanowires electrical resistance by a pseudo four-wire method, namely, by connecting each of the two leads with two wires in connection with the electronics. For our particular purpose of measuring the proximity effect, we also care about the resistive

transitions of the electrodes. The three-lead geometry provides great convenience for measuring the resistance of the front electrode by flowing current through the two side leads. Two independent measurements of either the nanowire or the front electrode can be done with one run without taking the sample out of the low-temperature chamber.

As the single nanowire contact with the front electrode is very fragile and sensitive to vibrations, temperature change, and pressure change, it is important to measure the sample right after the fabrication process. For resistive measurements in the physical property measurement system (PPMS), the sample has to be mounted onto a puck and wires have to be connected to voltage and current leads. After customizing the puck geometry and leads configuration, three samples can be directly plugged into build-in sockets which are always connected to the designated leads. With these efforts, the sample transportation and assembling process was usually done within 10 minutes.

Resistance measurements inside the PPMS (Quantum Design Inc.) were carried out according to the written measurement sequence. The measurement current was set to 0.1 μA to exclude heating effects. It is much smaller than the critical current of the nanowires. Since the nano-contact was also found to be sensitive to sudden change of current or static voltage, a switch box was always used to short the samples outside the PPMS when electrical connections were initiated or changed during a measurement. Temperature control was achieved automatically by the PPMS, with a base temperature of 1.8 K. Magnetic fields up to 7 Tesla is provided by a superconducting magnet. By using different sockets in the puck, we can align the nanowires either parallel or perpendicular to the direction of the magnetic field.

I-V measurements were carried out by adding a small AC modulation (~0.1 μA) to the ramping dc current. The dynamic resistance was measured using a PAR 124 lock-in amplifier. Both the differential resistance, d*V*/d*I*, and the dc voltage *V* were be measured at the same time. Additional electronics instruments were placed on a rack and connected to the switch box when needed. In such measurements, PPMS was only used to control the temperature and the magnetic field.

3. TRANSPORT DATA: LOW TEMPERATURE ELECTRICAL RESISTANCE MEASURMENTS

In this section, an overview of the transport data is given for each type of the electrode-nanowire-electrode structures. Rather than drawing conclusions on each type of structure, a survey of interesting features will be made for the samples measured. Comparisons will also be made for some related structures. However, detailed analysis and comprehensive discussions will be described in Section 4.

Parameters for each type of structures include the materials of the nanowires (NW), the electrode materials, the length of the nanowires (determined by the thickness of the membranes being used), and the diameters of the nanowires. Excluding the diameter as a variable, we have 14 types of structures. In total, we have successfully measured 167 samples.

The resistance of a sample was measured using the front and the back electrodes as the leads. Actual measurements were done with each electrode connected to two measuring wires in a "pseudo" four-probe configuration to eliminate the resistance of the measuring wires. The resistances measured at room temperature were typically in good agreement with the expected resistance values for single NWs calculated using the dimensions of the NWs and the bulk resistivity ρ of the materials at room temperature. The resistance of a typical film electrode was less than 0.1 Ω.

The resistance R of single Zn, Sn, and Pb NWs was measured down to 1.8 K in a Quantum Design physical properties measurement system (PPMS). The T_c of bulk Pb, Sn, and Zn are, respectively, T_c(Zn) = 0.88 K, T_c(Sn) = 3.7 K, and T_c(Pb) = 7.2 K [68].

3.1 Lead (Pb) nanowires

For Pb nanowires, we only have two choices of electrode materials due to the constraint by the chemical reactivities of Zn and Sn electrodes in Pb^{2+} contained solutions. It is not possible to fabricate Pb nanowires using Sn or Zn electrodes. The two possible choices are Au/PbNW/Au (Pb nanowires with Au electrodes) structure and Pb/PbNW/Pb (Pb nanowires with Pb electrodes) structure. In these structures, we can fabricate either long wires (60μm) or short wires (6μm), by using different thickness molecular membranes, anodic aluminum oxide (AAO) or polycarbonate (PC), respectively. We have measured a total of 42 samples.

3.1.1 Au/PbNW/Au

For all of the short nanowire samples we have measured, the normal Au electrodes were found to fully suppress superconductivity in the short Pb NWs inside the PC membrane. As shown in Fig. 3.1, samples showed no sign of superconductivity below 7.2 K, the T_c of bulk Pb.

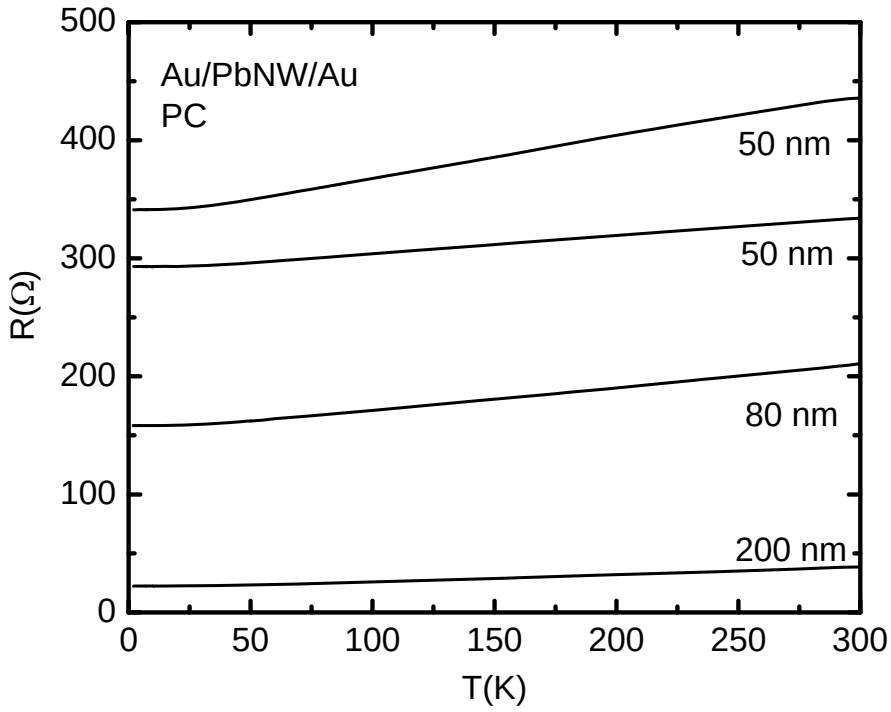

FIG. 3.1. The dependence of resistance on temperature in short (6μm) Pb NWs connected by two Au electrodes. Diameters of NWs are indicated

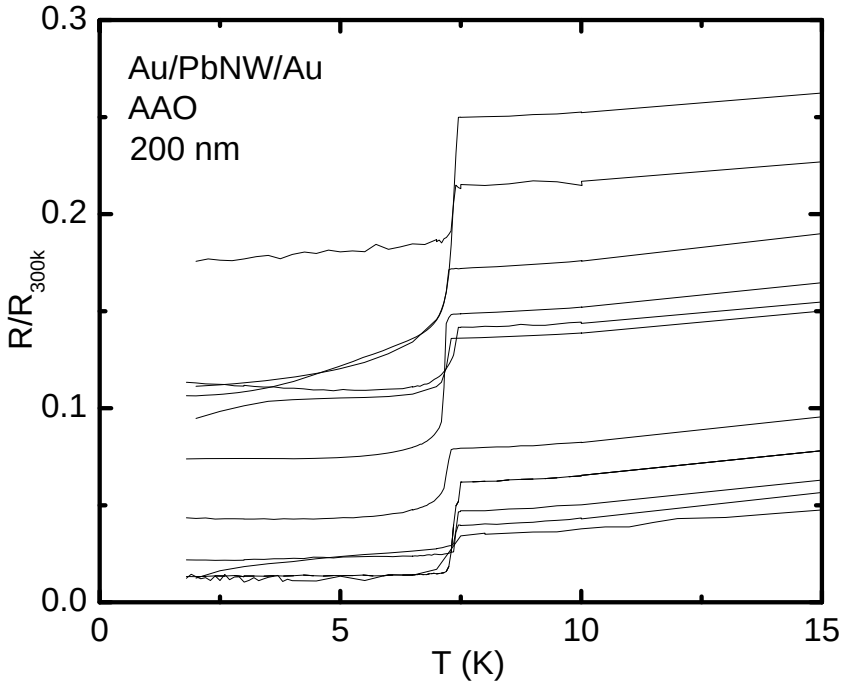

FIG. 3.2. The dependence of resistance on temperature in long (60μm) Pb NWs connected by two Au electrodes. Resistance data showed are normalized respect to their values at 300 K

Compared with the complete suppression of superconductivity in shorter Pb NWs, longer Pb NWs in AAO membranes showed partial suppression of superconductivity by the gold electrodes. From the measured resistance versus temperature data (*R*-*T* curves), we plot as a function of the temperature in Fig. 3.2 the resistance of the samples normalized by their values at room temperature (300 K). All the 27 samples we have measured displayed a superconducting transition at the transition temperature of bulk Pb T_C(Pb) = 7.4 K, but all had significant residual resistance below T_C(Pb) The Au electrodes only partially suppressed superconductivity in the long Pb NWs.

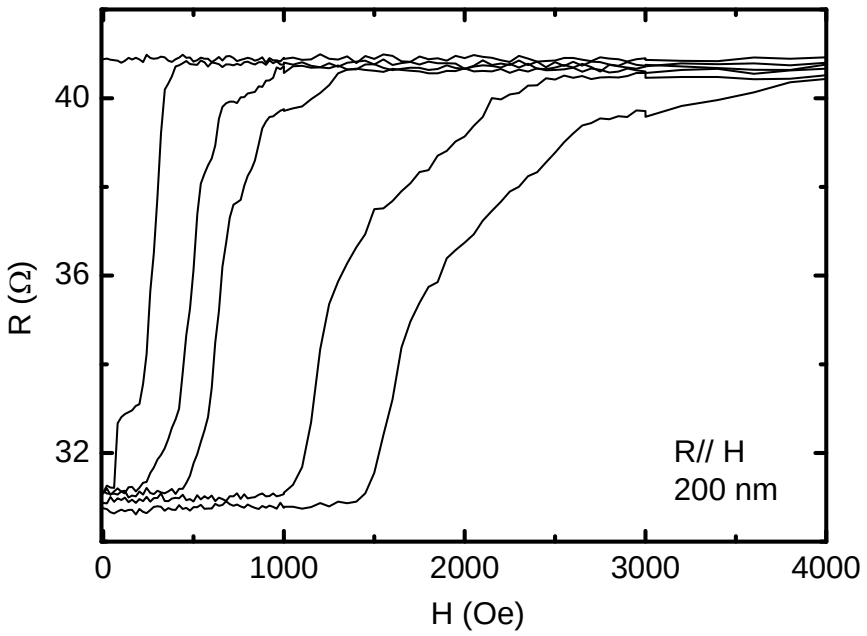

FIG. 3.3. Resistance dependence of an Au/PbNW/Au (60μm) sample under magnetic fields. *R-H* curves were measured with NWs parallel to the field direction at 2K, 4K, 6K, 6.5K, 7K and 7.5K, from right to left, respectively

We have also measured the field dependence of the resistance for each sample at low temperatures. They share similar features in terms of the shape of the curve and the critical field value. Instead of a sharp transition as observed in bulk Pb samples, we observe a continuous change of the resistance around certain fields. The value ranges from 1500 Oe to 4000 Oe at T = 2 K. At lower dimensions, the original Type I superconductor (Pb) tends to change to a Type II superconductor as found by many works [37, 69, 70]. Our data clearly show such a trend as we changed the NW diameters.

In addition to the temperature dependence of the resistance, extensive measurements of the *I-V* characteristics were also carried out. For all the samples, we have observed two types of *I-V* curves as shown in Fig. 3.4. The representative data in the top two graphs shows typical features of a weak superconductor: a rounded transition around the critical current (I_c) and a small value of I_c. The bottom graphs show the other type of *I-V* curves with robust critical currents. These two types of *I-V*s give critical current values differ by an order of magnitude. Both types of dc *I-V*s have a finite slope at zero current, consistent with the non-zero residual resistance. The top one doesn't have the sharp transition and the hysteretic feature depending on the current sweeping direction, in comparison with the features seen in the bottom one. We have also observed such features in other types of samples and will discuss in more details in later sections. For the ac *I-V*s, the top one shows a series of peaks. Detailed studies showed that the positions of these peaks move when the temperature or the applied field was changed [71]. This feature is similar to those reported elsewhere in other proximity-induced superconducting nanowires [72-74]. Such peaks are believed to be resulted from multiple Andreev reflections (MAR) at the normal-superconductor interfaces [54, 75, 76].

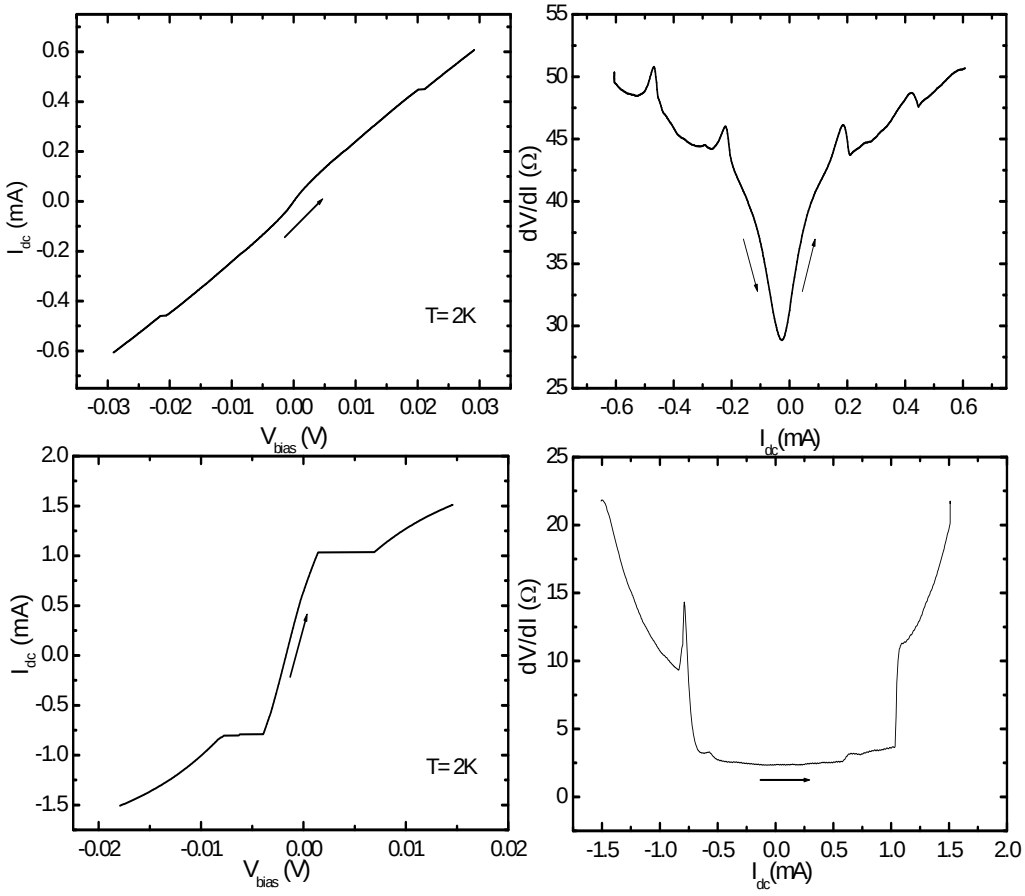

FIG. 3.4. Two types of *I-V* characteristics represented by two long Au/PbNW/Au samples with diameters equal to 200 nm. Top: ac (left) and dc (right) *I-V*s of one sample; Bottom: dc (left) and ac (right) *I-V*s of another sample; Arrows indicate current sweeping directions

3.1.2 Pb/PbNW/Pb

Pb nanowires between two Pb electrodes display the expected behavior. Both long (60μm) and short (6μm) wires show complete superconductivity with zero resistance

below the bulk Pb transition temperature. Most samples we have measured were long Pb NWs. We plot the representative data in Fig. 3.5.

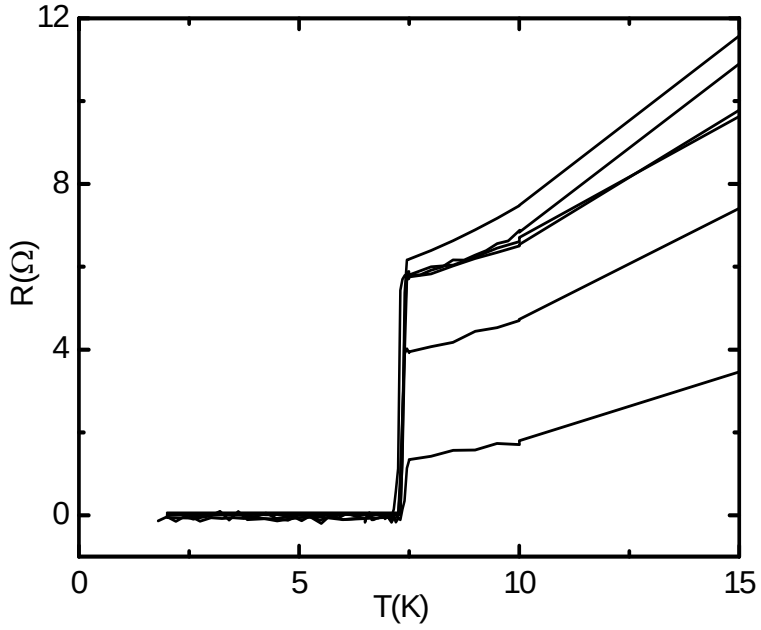

FIG. 3.5. *R-T* data of Pb/PbNW/Pb samples with nanowires have length of 60μm. Diameters of nanowires are all 200 nm

We have also measured the field dependence and *I-V*s for these samples. As a typical example, Fig 3.6 shows *R-H* cures and dc *I-V* curves at various fields and temperatures. With a zero resistance state below the bulk Pb transition temperature, Pb NW showed the behavior of a type II superconductor in a magnetic field.

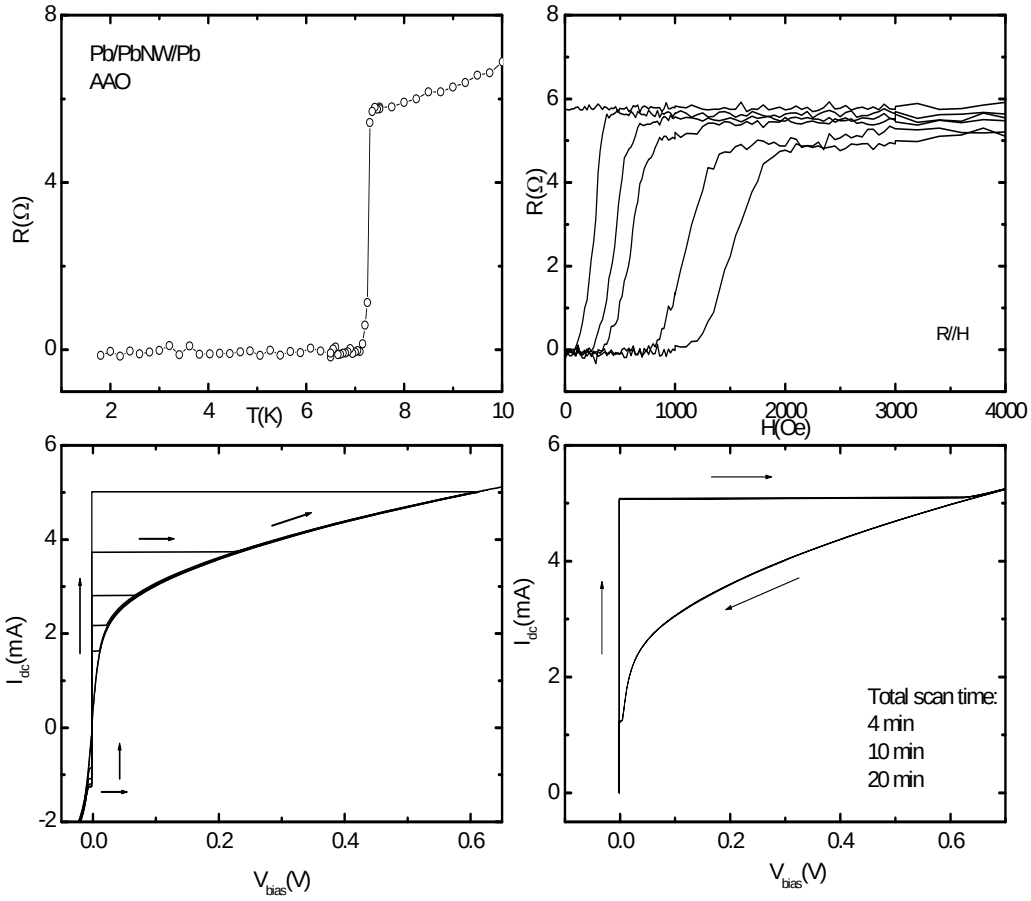

FIG. 3.6. Transport data of a Pb/PbNW/Pb sample with length of the nanowire equal to 60 μm. Top: *R-T* and *R-H* curves at *T*= 2,4,6,6.5,7,7.5 K from right to left; Bottom: *I-V* curves at *T*= 2,3,4,5,6,7, 7.2 K (left) and ramping rates at 2K (right)

Dc *I-V*s were also measured for this sample at various temperatures, as shown in Fig. 3.7. A significant hysteresis was observed in the long Pb/PbNW/Pb sample. *I-V* hysteresis has been also reported in other systems [75, 76] and is often attributed to Joule heating [37]. However, by changing the ramping rate of the current as we did for this

sample and also by staying for different periods of time at the high current regime, we didn't find any measurable change in the hysteresis. This suggests that the hysteresis is not due to heating.

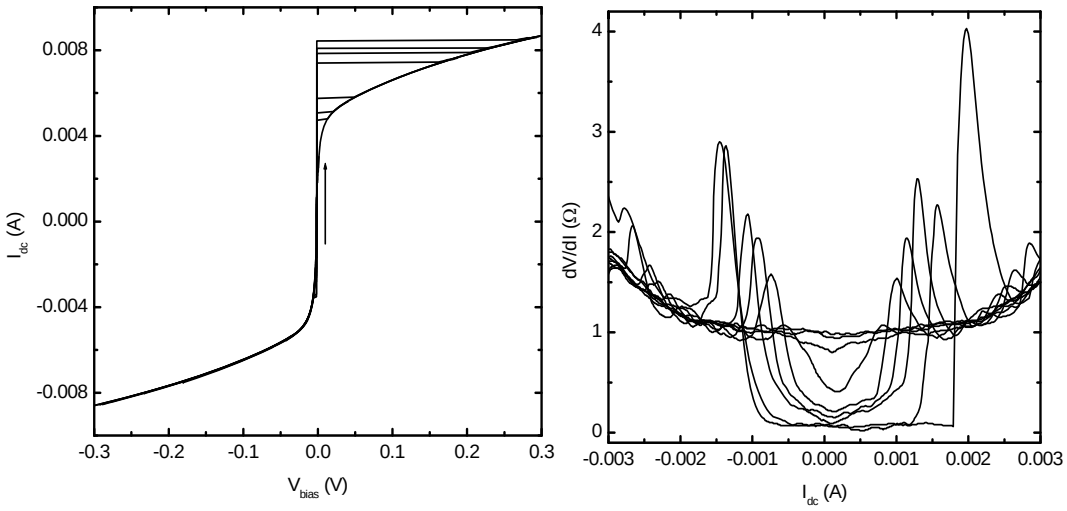

FIG. 3.7. Dc and ac *I-V*s for long Pb/PbNW/Pb sample. (Left) dc *I-V*s at *T*= 2K under magnetic fields of 0, 200, 400, 450, 500, 550, 600, 800, 850 Oe; (right) ac *I-V*s at *T* = 2K under fields of 500, 850, 1000, 1050, 1100, 1200, 1400, 1600, 1800 Oe; all fields were parallel to the wire

*I-V*s measured at 2 K with at various magnetic fields show similar features as those measured at various temperatures. With increasing fields in Fig. 3.7, the critical current becomes smaller and the transition becomes smoother. At the same time, the hysteresis due to sweeping direction also becomes less significant. From the ac *I-V*s, the sharp and one step transition gradually becomes multi-peak and smooth ones. Namely, we have

observed both types of *I-V*s in Fig. 3.4 for this sample, as superconductivity was destroyed by either increasing the magnetic field or raising the temperature.

3.2 Tin (Sn) nanowires

For Sn nanowires, we have three choices of electrode materials to form Au/SnNW/Au, Sn/SnNW/Sn and Pb/PbNW/Pb structures. We can fabricate either long wires (60μm) or short wires (6μm), by using different molecular membranes, anodic aluminum oxide (AAO) or polycarbonate (PC), respectively. We have measured a total of 81 samples.

3.2.1 Au/SnNW/Au

For Sn NWs with Au electrodes, we have obtained results that are similar to those observed in Pb NWs. For short wires, the Au electrodes fully suppressed superconductivity in the Sn NWs, as shown in Fig. 3.8.

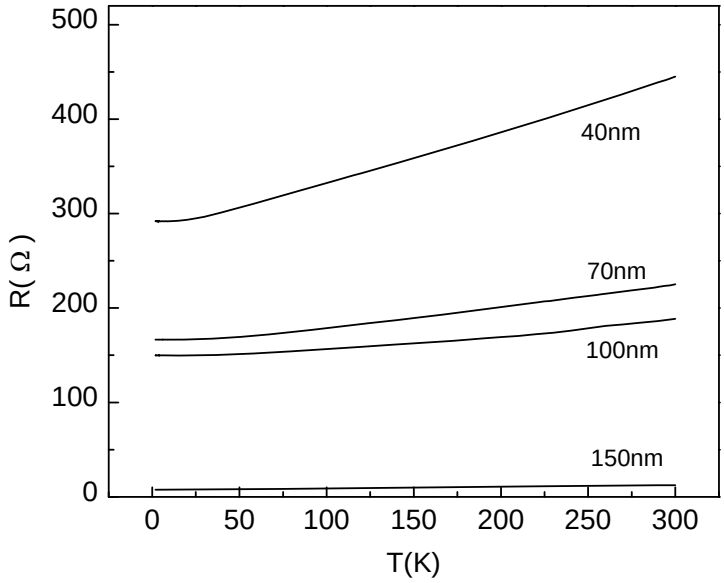

FIG. 3.8. *R-T* data for four short Sn nanowires grown between two Au electrodes. Diameters of NWs are indicated

On the other hand, a partial suppression of superconductivity by Au electrodes was observed in long Sn NWs. *R-T* data of three samples in Fig. 3.9 clearly show that all of them had significant residual resistance below the transition temperature, which kept decreasing as temperature was lowered further. The normalized resistance data in the inset shed light into the behavior of samples related to their residual-resistance-ratio (RRR). The inverse of the R/R_{300K} value gives the RRR. Comparing the three samples, we found that samples with larger RRR values had larger values of non-zero resistance ratio below the transition temperature. Further discussions about RRR and the proximity effect will be presented in Section 4.

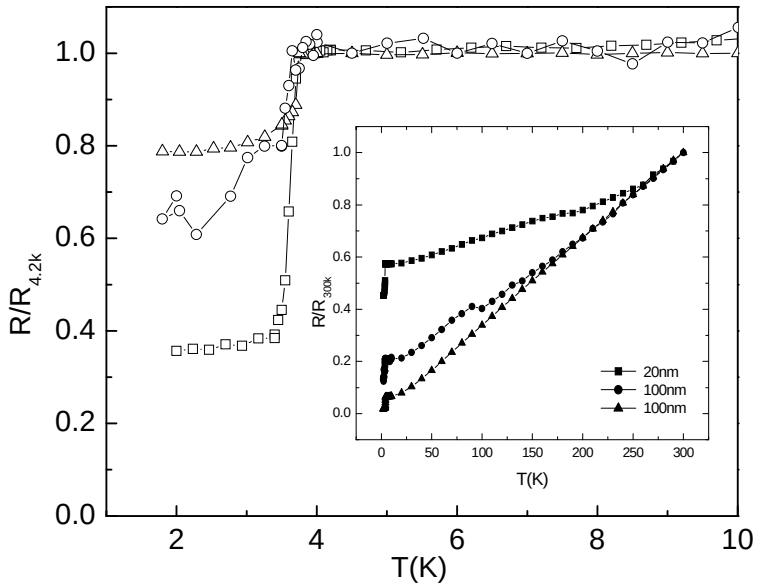

FIG. 3.9. Resistance data of long Sn nanowires grown between Au electrodes. Resistance of all three samples were normalized to their values at 4.2 K; Inset: resistance data normalized to their values at 300 K for the same three samples

*I-V*s in long Sn NWs with Au electrodes can also be classified into two categories: one with sharp transitions and one with smooth transitions, as shown in Fig. 3.10. Interestingly, none of the measured *I-V*s showed hysteretic behavior. Both the ac *I-V* and dc *I-V* curves give transitions at a critical current I_c. Ac *I-V*s show peaks corresponding to the slope change in the dc *I-V*s. However, as we can see for both samples, the sharpness of the transition is quite different. If a sharp transition suggests a robust superconducting state, the rounded transition in the second sample in the bottom figure suggests a relatively weak superconducting state. Currently, we don't have a clear

understanding of what contributes to the difference. We have observed both cases in different samples having the same structure.

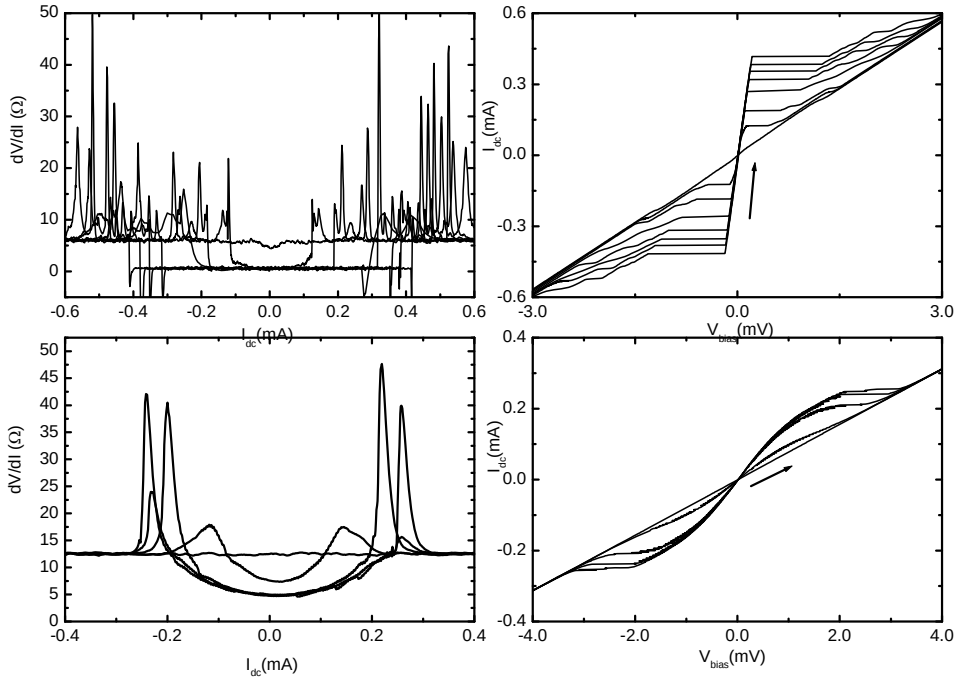

FIG. 3.10. *I-V* characteristics of two types of Au/SnNW/Au structures with long nanowires. Top: Ac (left) and dc (right) *I-V* curves of one sample at T = 2, 2.5, 2.75, 3,3.25, 3.5, 3.75 K with decreasing critical current; Bottom: ac (left) and dc (right) *I-V* curves at T = 2 K under magnetic fields of 0, 100, 200, 400, 800 Oe with decreasing critical currents

3.2.2 Sn/SnNW/Sn

We have also studied both long and short Sn NWs grown between Sn electrodes. As expected, both types showed complete superconducting transitions to zero resistance below the bulk transition temperature of Sn. *R-T* curves of several Sn/SnNW/Sn

structures in PC membrane are presented in Fig. 3.11. Normalized resistance drops to zero below T_c(Sn).

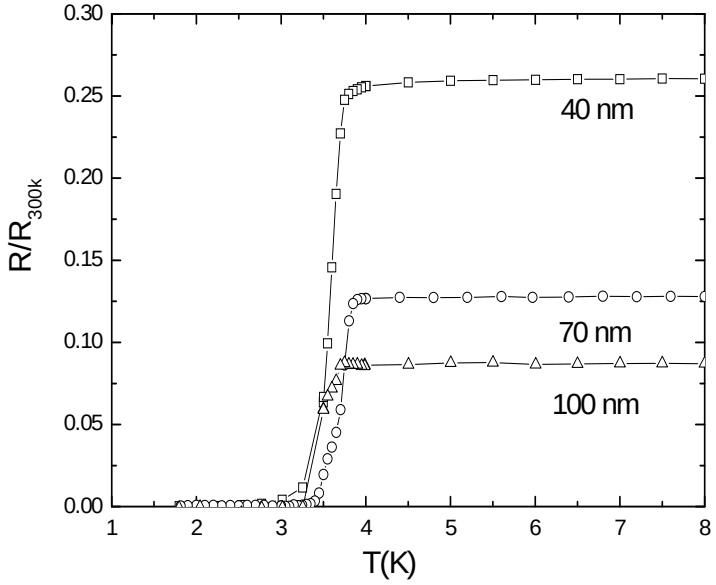

FIG. 3.11. Resistance versus temperature data of short Sn NWs between Sn electrodes. *R* values were normalized to those at 300 K

We have also measured the field dependence of the resistance and *I-V* curves on many Sn/SnNW/Sn samples. Fig. 3.12 shows the data from one typical Sn/SnNW/Sn sample. The *R-T* curve shows a clear and sharp transition from 50 Ohms to 0 at the bulk Sn transition temperature, 3.7 K.

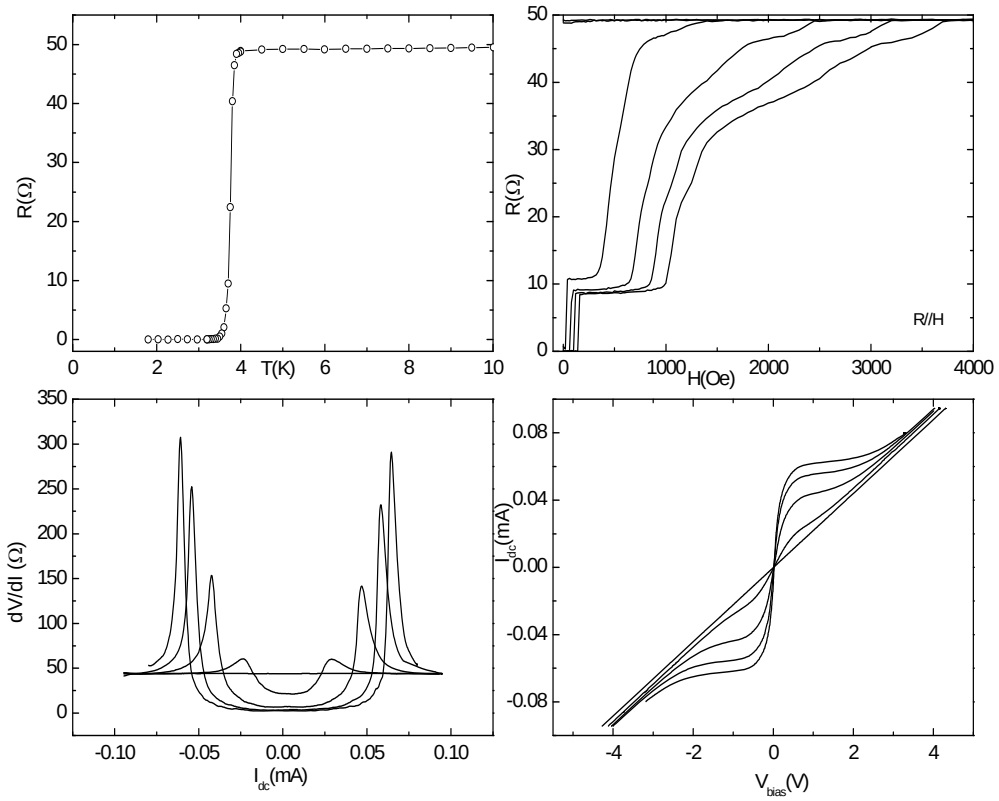

FIG. 3.12. Transport data of a short Sn/SnNW/Sn sample. Top: *R-T* curve and *R-H* curves from left to right; *R-H* curves were measured at *T*= 2, 2.5, 3, 3.5, 4, 5 K from right to left; Bottom: ac and dc *I-V* curves at *T* = 2, 2.5, 3, 3.5, 4 K with decreasing critical current

The critical field of the nanowire is estimated to be about 0.1 T from the *R-H* curves measured below T_c. The nanowire showed a typical Type-II superconductor behavior with H_c far greater than that of the bulk Sn metal. We have also observed a jump in the resistance at a small field of 200 Oe which agrees well with the critical field of the Sn electrode measured independently. This jump is consistent with the proximity effect

because as the thin film electrode is driven to normal at the critical field, part of the nanowire sample is also brought to the normal state due to the inverse proximity effect. Since the wire is only 6 μm long, the normal portion can change significantly the resistance value of the entire system. However, such an effect in long nanowires is not so significant since the length of the normal part affect by the electrode is only a small portion of the total length. This is clearly shown in Fig. 3.13 as the inset. All of the samples show a zero resistance below the bulk Sn transition temperature.

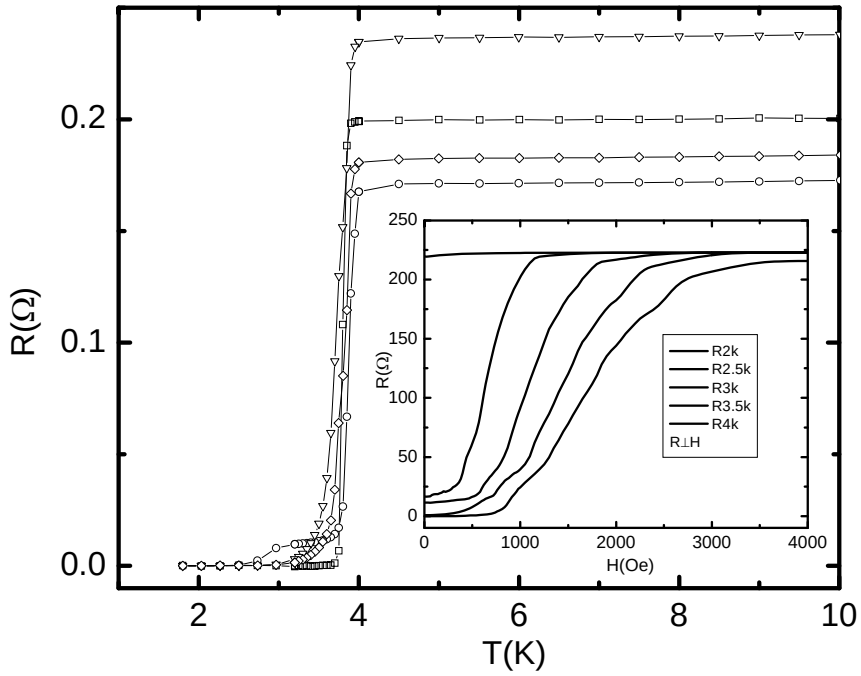

FIG. 3.13. Resistance-temperature data of long Sn NWs grown between Sn electrodes. Inset: *R*-*H* curves of one sample at T = 2, 2.5, 3, 3.5, 4 K from right to left

3.2.3 Pb/SnNW/Pb

The data for Pb/SnNW/Pb show clearly a long-range proximity effect. The Sn NWs become superconducting right below the T_c of the Pb electrodes. For all the 8 short and 13 long Pb/SnNW/Pb structures we have measured, the proximity-induced superconducting state shows a zero resistance below T_c(Pb), as shown in Fig. 3.14. The R-H curves all show a significant jump at the critical field of the Pb electrodes, which is about 0.1T at 2K [77].

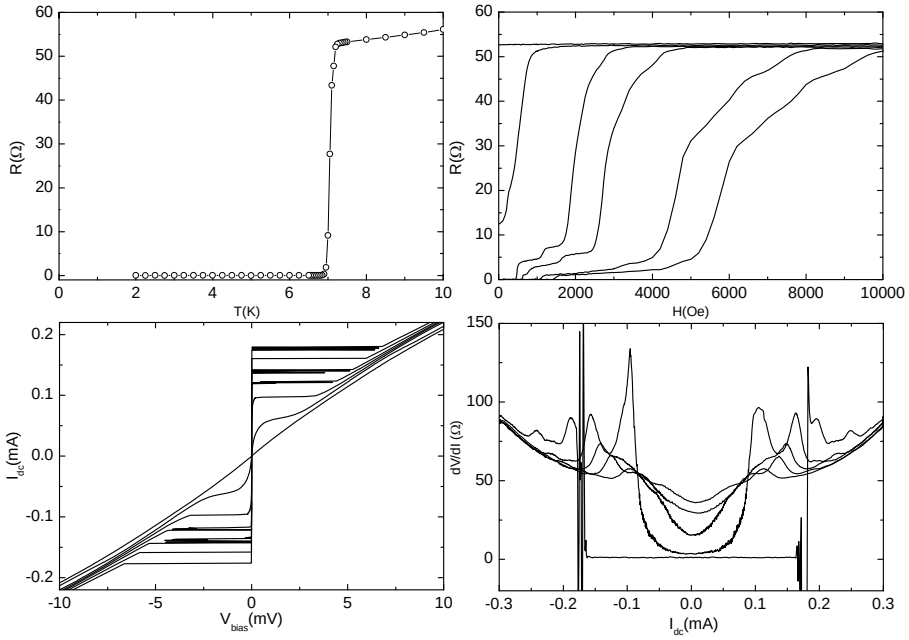

FIG. 3.14. Transport data for a short Pb/SnNW/Pb sample with diameter of the nanowire equal to 100 nm. Top: *R-T* (left) and *R-H* (right) curves, *R-H* were measured at *T*= 2, 4, 6, 6.5, 7, 7.5 K with field perpendicular to the wire; Bottom: dc *I-V* curves at *T* = 2, 4, 5, 5.5, 6, 6.5, 7 K with decreasing critical currents (left); Ac *I-V* curves measured at *T* = 2K under magnetic fields equal to 0.2, 0.4, 0.5, 0.6, 0.7 T with decreasing critical currents

The *I-V* curves of the sample in Fig. 3.14 do not show a hysteretic behavior, although the transition was sharp. In the ac *I-V*s, we observe a continuous change from sharp, one-peak transitions to more continuous, multi-peak transitions. This indicates that those samples which only have smooth transitions at low temperatures may have a superconducting state that has been already compromised by either physical structure or the environment, even before applying any external magnetic field.

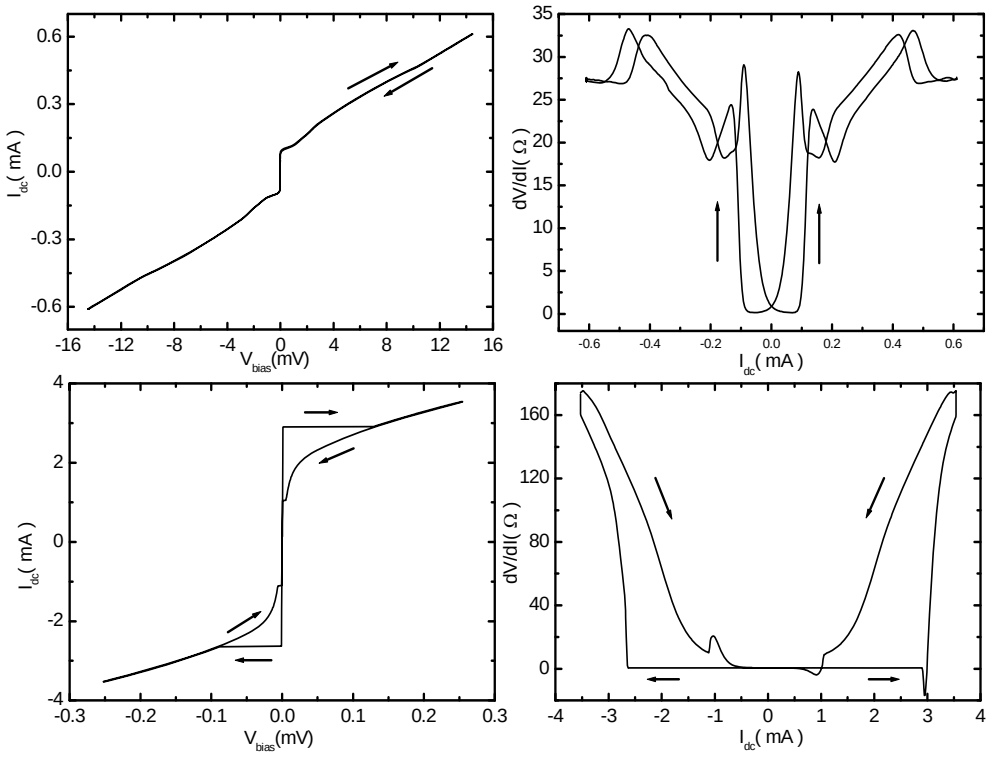

FIG. 3.15. Dc (left) and ac (right) *I-V* curves of two Pb/SnNW/Pb samples with length of the nanowires equal to 60 μm. Arrows indicate current sweeping directions. These *I-V*s were measured at $T = 2$ K with dc and ac *I-V*s measured simultaneously

For long Sn nanowires, besides the difference in the *R-H* curves as we have shown for long Pb wires, we have also observed two types of *I-V* characteristics. An example is shown in Fig. 3.15 for one type at the top and the other at the bottom. Besides the apparent different order of magnitude of the critical current (more than ten times), the top one doesn't show any significant hysteretic behavior as is seen in the dc *I-V*s at the bottom.

3.3 Zinc (Zn) nanowires

Since the transition temperature of bulk Zn is 0.85 K, we can only measure superconducting properties of them by using dilution refrigerator instead of the PPMS. For the electrodes, we can choose Au, Pb, Sn or Zn. However, because the complication of using the dilution refrigerator system, only several samples survived the long cooling down process after trying many times. The measurement of two long Au/ZnNW/Au samples was successful and a sharp transition in dc *I-V* curves was recorded below T = 0.85 K. Our effort was focused on the proximity-induced superconductivity, in Sn/ZnNW/Sn and Pb/ZnNW/Pb samples.

3.3.1 Sn/ZnNW/Sn

For all the 8 long and 12 short Zn NW samples we have measured, superconductivity was observed below the T_c = 3.7 K of bulk Sn. Interestingly, in addition to many samples that have zero resistance below the transition, we have also observed some cases in both short and long nanowire samples display a non-zero resistance below the transition temperature. We show the *R-T* data for samples of both short and long Zn

nanowires in Fig. 3.16. Normalized resistance of the samples showed different behavior below transition temperature, indicating that the electrodes have different effects on the Zn NWs. In other words, the proximity effect has different strength among otherwise similar samples. Similar to those observed in Fig. 3.9 for long Au/SnNW/Au samples, the RRR plays a systematic role for determining the strength of the proximity effect. More discussions will follow in Section 4.

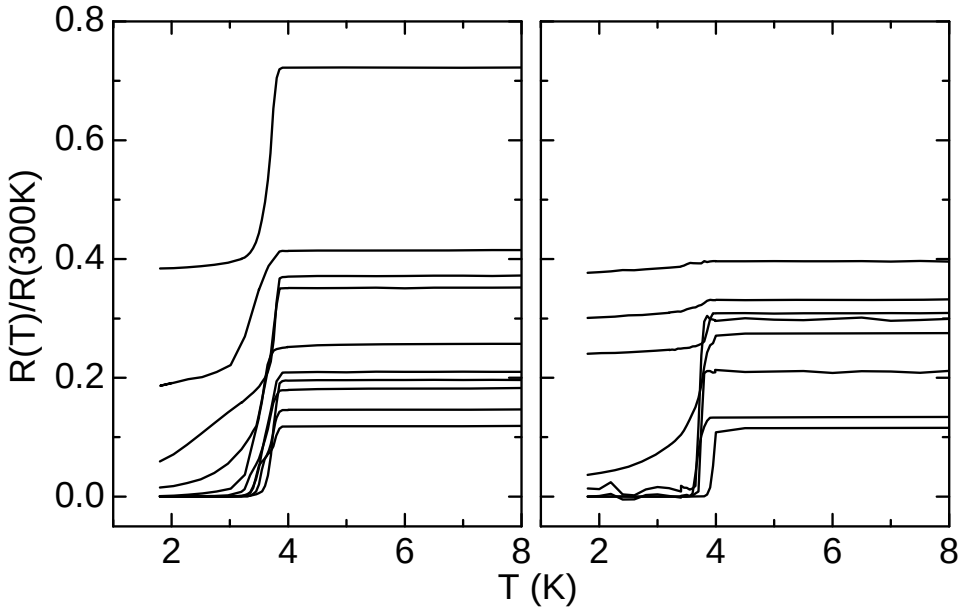

FIG. 3.16. *R-T* curves for short (left) and long (right) Zn nanowires in between two Sn electrodes. Resistance was shown after normalized to their resistance at 300 K

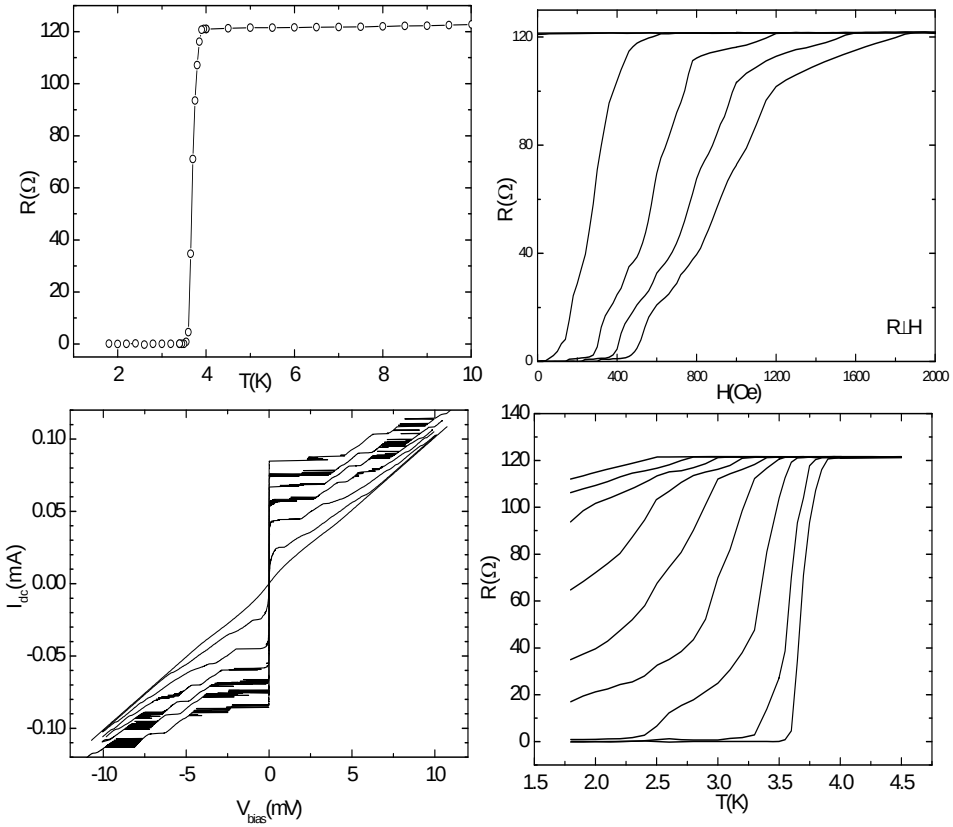

FIG 3.17. Transport studies of a Sn/ZnNW/Sn sample with length of the nanowire equal to 60 μm. Top: *R-T* and *R-H* curves measured at T = 2, 2.5, 3, 3.5, 4, and 5 K, from right to left. Bottom: (left)dc *I-V* curves at T= 2, 2.5, 2.75, 3, 3.25, 3.5, 3.7 K as curves moves to the center; (right) *R-T* curves under fields of 0, 200, 400, 600, 800, 1000, 1200, 1400, 1600 Oe from right to left

As a typical example, we show the transport data for a Sn/ZnNW/Sn sample in Fig. 3.17. Induced superconductivity is observed in the 60 μm-long nanowires. The long Zn NW has a zero resistance below the transition temperature of the Sn electrode. However, as we noticed in the *R-H* curves, the resistance jump at low field shifted and become less

prominent than those in the short wires. This becomes clear after we measured the critical field values of the thin film electrodes. We found that the critical field of the film electrode also changed to higher values possibly due to more and bigger holes in the film and can be as large as 0.1 T for Sn films.

The *I-V*s of this system show a new feature as shown in Fig. 3.17, with many steps in the dc *I-V* curves as the temperature or the magnetic field was changed. The steps are accompanied by oscillations between two adjacent states. These can be attributed to the formation of phase-slip centers (PSC) [48] along the nanowire as we describe in details later.

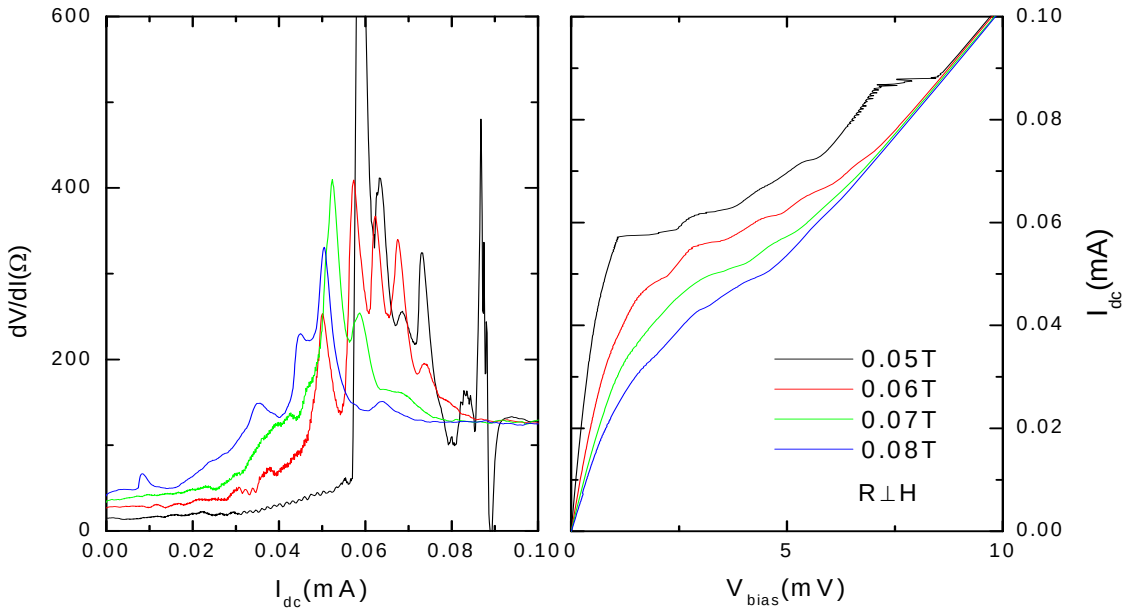

FIG. 3.18. *I-V* characteristics of the same Sn/ZnNW/Sn sample. Dc (right) and ac (left) *I-Vs* with changing magnetic fields at T=2K

In the ac *I-V* curves for the same sample in Fig. 3.18, we found the existence of both sharp peaks correspond to the sharp dc *I-V* transitions and multi-peak feature corresponding to the region with a finite resistance value. This multi-peak feature resembles those found in wires with finite residual resistance as shown in Fig. 3.4 for long Au/PbNW/Au samples. This feature suggests the existence of normal parts along the wires below the transition temperature.

3.3.2 Pb/ZnNW/Pb

We have measured two short Zn NWs grown between Pb electrodes as shown in Fig. 3.19. Field dependence data and *I-V*s for one sample are also presented. With the short sample showing a significant resistance jump around 0.1 T at T = 2K, we can further confirm the relation of such a feature to the wire length. The *I-V* characteristics are very similar to those measured in Pb or Sn NWs with Au electrodes. Namely, they both have the smooth transition and the multiple peaks feature. Knowing the zero-resistance state below the transition, we conclude that the zero-resistance superconducting states observed in *R-T* curves may have various behaviors in *I-V*s. These measurements tend to give more information about the robustness of the superconducting state.

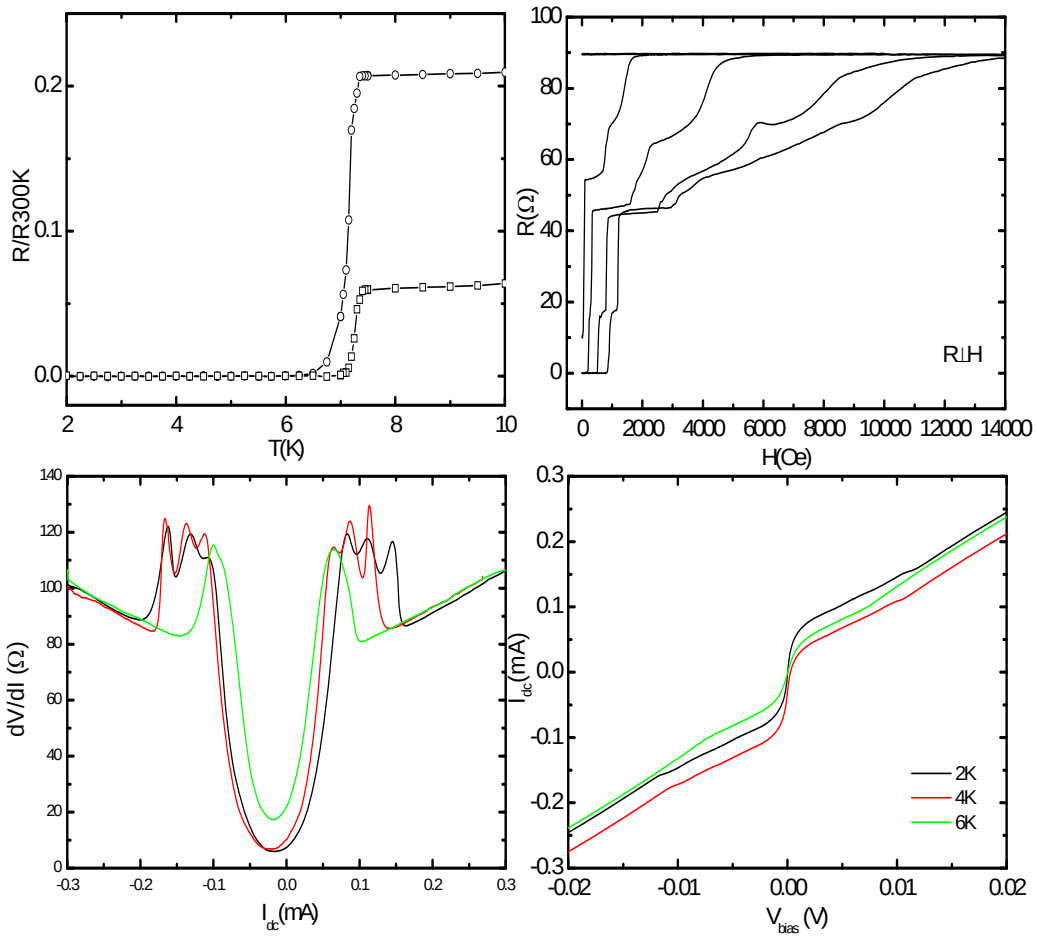

FIG. 3.19. Transport data of short Pb/ZnNW/Pb samples. Top: (left) normalized resistance-temperature data for two samples; (right) *R-H* curves at *T*= 2,4,6,7,7.5,8 K for one sample; Bottom: ac (left) and dc (right) *I-V*s for the same sample with color indicateing different temperatures

Proximity-induced superconductivity in a 60 μm range was fully observed in Pb/ZnNW/Pb structures made with AAO membranes. *R-T* data from 22 samples that we have measured are plotted in Fig. 3.20. Interestingly, we found many samples have a

non-zero resistance below the transition at 7.2 K, similar to those observed in Sn/ZnNW/Sn structures.

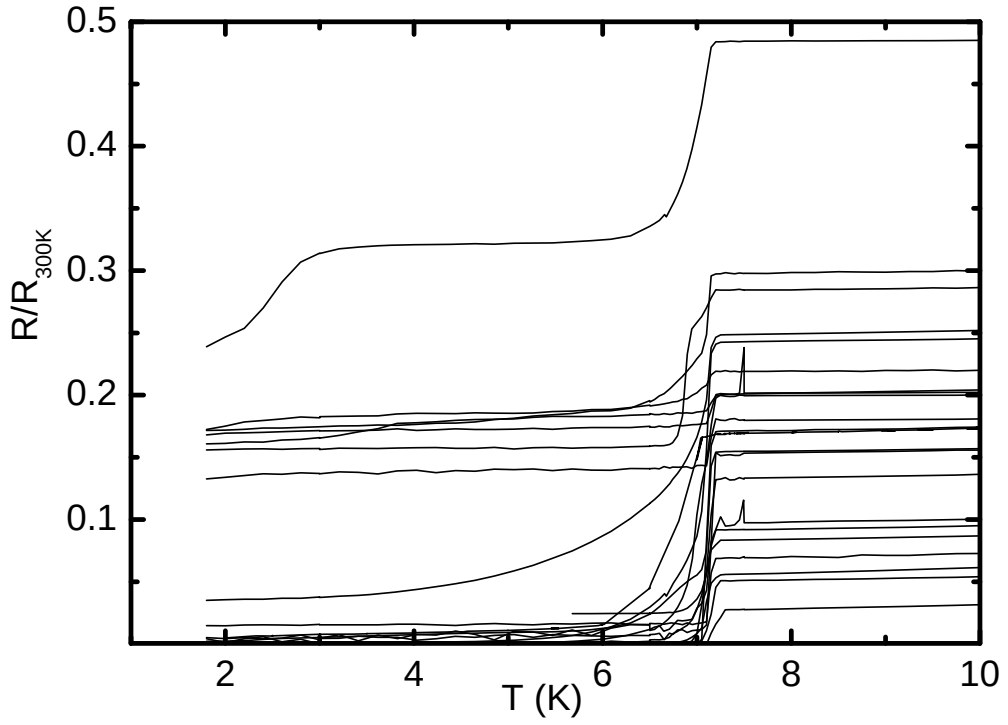

FIG. 3.20. Resistance versus temperature data of long Pb/ZnNW/Pb samples. Resistance is normalized to their values at 300 K

We have tried to measure such samples in a dilution refrigerator to investigate the transition near transition temperature of bulk Zn. However, the samples which finally survive to the temperature range all happened to have zero resistance below the Pb electrode transition, 7.2 K. Many *I-V*s have been successfully measured. With features similar to those observed in long Sn/ZnNW/Sn samples, we have recorded a number of

systematic steps in the dc *I-V* curves as those presented in Fig. 3.21. Such a feature was observed in all the long NWs described previously.

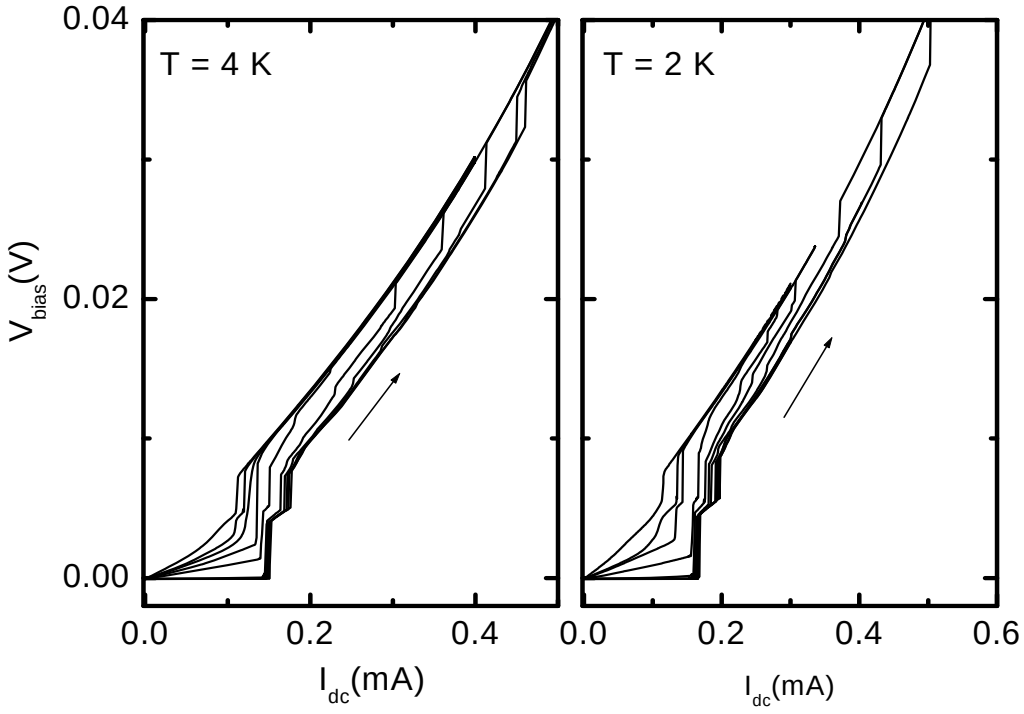

FIG. 3.21. Dc *I-V*s of a Pb/ZnNW/Pb sample with length of the nanowires equal to 60 μm. left: dc *I-V*s at *T* = 4K under magnetic fields of 0, 200, 400, 600, 800, 1200, 1600, 1800, 2350, 3000 Oe, from right to left; Right: dc *I-V*s at T = 2K under fields of 0, 500, 800, 1000, 1150, 1500, 2500, 3000, 5000 Oe, from right to left

The phenomenon is explained in terms of the induction of phase-slip centers (PSC) along the nanowire, as established in earlier years to explain similar feature in

superconducting micro-bridges and constrictions [49, 78]. By changing the temperature and the magnetic field, PSCs can be generated one after another along the wire. With available data from the *I-V* curves, we can estimate the size of such PSCs, as we will describe in Section 4.

4. DATA ANALYSIS: PROXIMITY-INDUCED SUPERCONDUCTIVITY IN SINGLE-CRYSTAL NANOWIRES

In this section, we summarize the transport measurement results and present our primary data analysis based on all the data we have obtained. Since there are many features of the phenomena, the analysis will be organized with different focus in each subsection. Nevertheless, all of these different perspectives are inter-related.

4.1 Long-range proximity effect

Electrode-induced superconductivity is the obvious conclusion based on the resistance (R) versus the temperature (T) data. This proximity effect is reflected by two types of observations. Namely, the suppression of superconductivity in superconducting (Pb, Sn) nanowires by normal metal (Au) electrodes and the induction of superconductivity in Sn and Zn nanowires above their respective bulk superconducting transition temperatures by superconducting electrodes having higher transition temperatures. Both observations are clearly demonstrated in Fig. 4.1, where R-T data from samples having different nanowire/electrode combinations are plotted together.

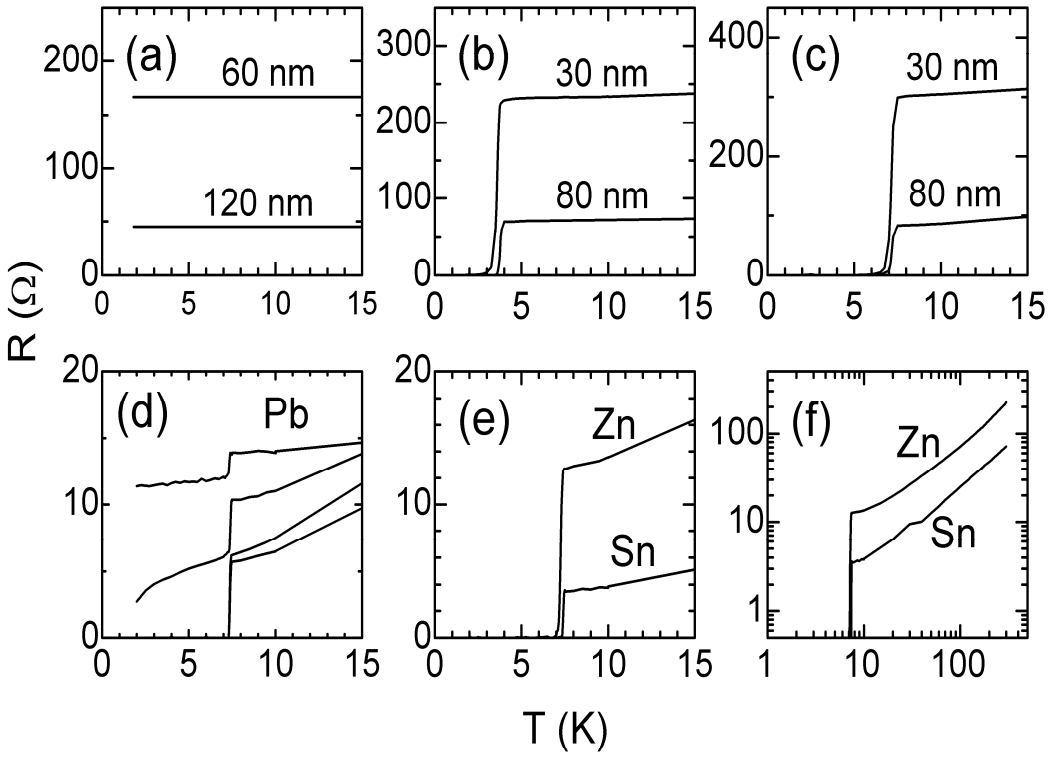

FIG. 4.1. Proximity effect observed with *R*-*T* curves of various structures. Top: *R* vs. *T* for 6-μm-long Sn NWs of indicated diameters with electrodes of (a) Au, (b) Sn, and (c) Pb. Notice that superconductivity is suppressed with Au electrodes, but with Sn or Pb electrodes Sn NWs are superconducting at the respective T_c of the electrodes. Bottom: *R* vs. *T* for 60-μm-long NWs of d = 200 nm. (d): Partial suppression of superconductivity shown for Pb NWs with Au electrodes (upper two curves) and fully superconducting Pb NWs with Pb electrodes (lower two curves). (e): Superconducting at T_c(Pb) for Zn and Sn NWs with Pb electrodes. (f): *R* vs. *T* up to 300 K showing the large RRR values of Sn and Zn NWs

For 6-μm-long Pb and Sn NWs in contact with Au electrodes, we did not observe any signature of superconductivity down to 1.8 K, however, when 6-μm-long Zn or Sn NWs were in contact with superconducting electrodes having a higher T_c, they became superconducting at the T_c of the electrodes. This is shown by the top frames in Fig. 4.1 for Sn NWs. For 60-μm-long NWs, superconductivity in Pb and Sn NWs was only partially suppressed by Au electrodes as shown by Fig. 4.1 (d) for Pb NWs, yet, superconductivity induced by Pb electrodes in Zn and Sn NWs was robust, as shown by Fig. 4.1 (e). Fig. 4.1 illustrates a PE in NWs of up to 60 μm in length. These single crystalline NWs had large residual-resistance-ratios (RRR) values of up to 50, as shown by Fig. 4.1 (f).

Considering the traditional picture of proximity effect (PE) between a normal metal (N) and a superconductor (S), either the suppression or the induction effect in a long range can be achieved by making a clean S-N interface and high quality S/N materials [73, 79]. We believe that our samples, single-crystal nanowires with *in situ* contacts to the electrodes, are superior in both respects. However, normally, the proximity effect is bounded by the normal electron coherence/thermal length in the material [37, 58]. In the clean limit, the thermal length L_T is 2 μm at 7.2 K and 3.8 μm at 3.7 K for Sn and Zn, about half the length of 6-μm-long NWs. Therefore, coherence over the length L_T cannot be excluded as the origin of the PE in 6-μm-long NWs. However, it is much too short to account for the PE in 60-μm-long NWs. This long-range effect definitely calls for new physical pictures.

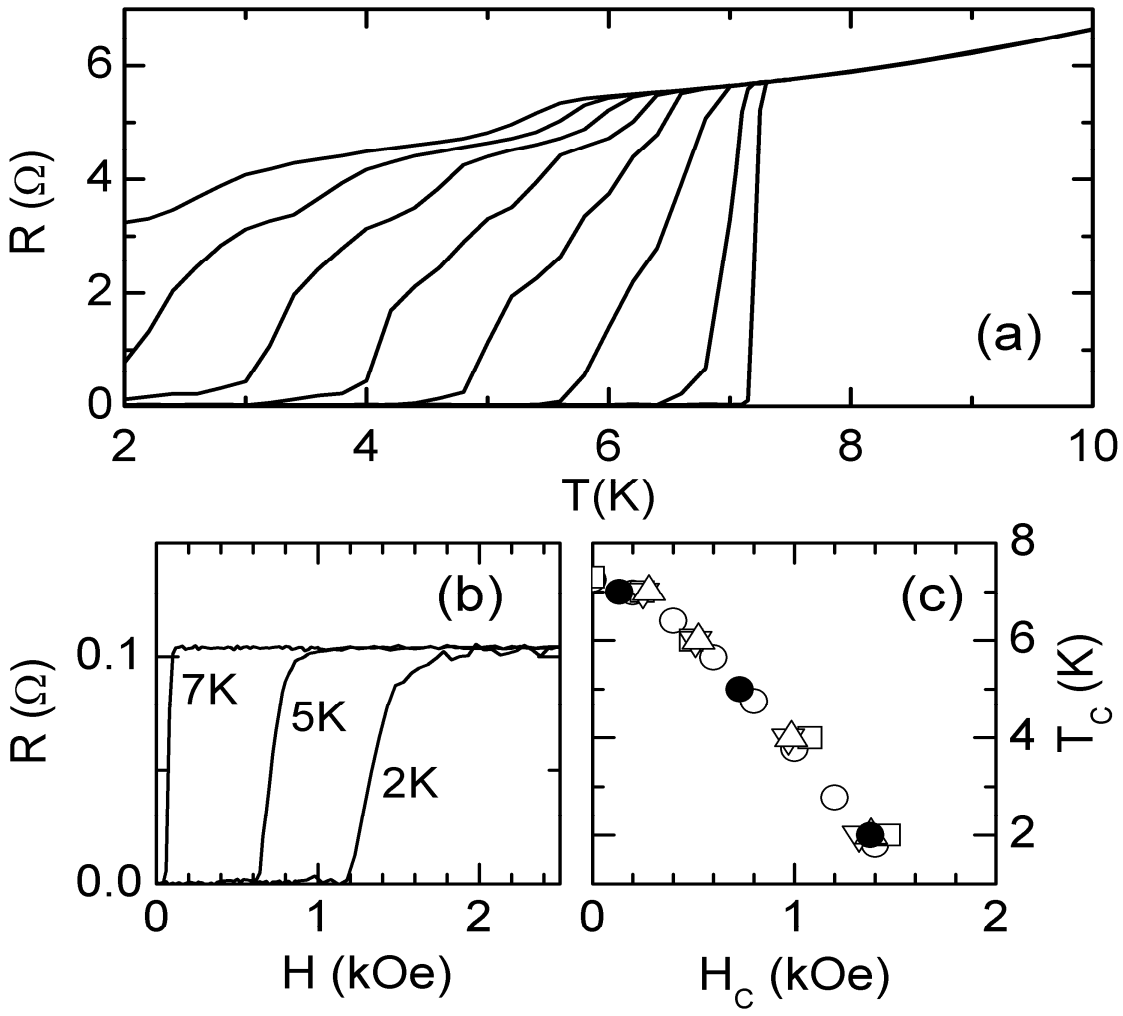

FIG. 4.2. Transport data of an electrode and nanowire with changing temperature and magnetic field. (a): *R* vs. *T* for a 60-μm-long Sn NW with Pb electrodes at transverse fields of 0, 0.2, 0.4, 0.6, 0.8, 1.0, 1.2, and 1.4 kOe for curves from right to left. (b): *R* vs. *H* in the same orientation for a Pb electrode at selected temperatures. (c): T_c or H_c determined from (a) in open circles and from (b) in filled circles. Other open symbols are from other 60-μm-long Sn NWs with Pb electrodes

This anomalous long-range PE was studied further by measuring the field dependence of the resistive transitions. We illustrate using a set of data from a 60-μm-long Sn NW (d=200 nm) grown with Pb electrodes. We plot the resistive transitions of the Sn NW (Fig. 4.2 (a)) and one Pb electrode (Fig. 4.2 (b)), with the field H applied transverse to the NW (parallel to the Pb film electrodes). We define T_c or the critical field H_c at the mid point of a transition. In Fig. 4.2 (c), we plot the H_c of the Pb electrode (solid circles) and the T_c of the Sn NW (open circles), showing consistently that the transitions of the Sn NW tracked that of the Pb electrode. Additional open symbols in Fig. 4.2 (c) were obtained from other Sn NW grown with Pb electrodes.

As we presented in Section 2, our structural and compositional analyses using SEM and TEM have clearly illustrated the structure of the electrode-nanowire-electrode structure and ruled out any measurable mixing of the electrode materials into the nanowires. Therefore, we are confident that our transport data have demonstrated the observation of an anomalous long range proximity effect.

As mentioned earlier, the unique contacting method we used is likely another contributing factor for such effect. Considering a cylindrical NW of diameter d forming an ideal contact with a perpendicular infinite plane of resistivity ρ, the resulting contact resistance $(\rho/2\pi)|\ln(d/2)|$ is negligible. We believe it is crucial to form virtually ideal contacts between a NW and the electrodes with a near perfect transparency at the interfaces. This is probably possible with our *in situ* method since electroplating is a reduction process which may effectively clean the oxide layer off the electrodes and produce an atomic-scale inter-diffusion layer at the interface. A near perfect

transparency at the interface is critically important if similar long-range proximity effects are to be reproduced in single-crystal NWs with electrodes fabricated using electron-beam lithography [60].

4.2 *I-V* characteristics and phase-slip centers (PSC)

The *I-V* data presented in Section 3 illustrate that they are a sensitive approach for detecting fine features in the superconducting state below T_c. As a good example, samples with a zero resistance below T_c may have critical current (I_c) varying by orders of magnitude. Many of our analyses of the *I-V* data have shined much light in understanding the proximity effect and many aspects of the superconducting states in the nanowires (NW).

The *I-V* data we have obtained from a variety of samples have covered a wide range in both characteristic features and values of the critical current. It is useful to define several key parameters to the *I-V* characteristics. They are: (1) The value of the critical currents at $T = 2$ K, I_c; (2) The sharpness of the transition in the dc *I-V* curves at the lowest temperature (2 K) and in zero external field; (3) The hysteresis in both the dc and the ac *I-V* curves when changing the sweeping directions of the current; (4) The voltage steps in the dc *I-V* curves corresponding to the phase-slip centers (PSC); (5) Single peak or multiple peaks structures in the ac *I-V* curves related to Andreev reflection at the S-N interface [80, 81].

One of the most interesting features in the *I-V* curves is the voltage steps observed in dc *I-V*s of many samples. This feature provides useful information for further

understanding the proximity effect. Approaching H_c, the *I-V*s showed reproducible and regular steps identical to those seen in superconducting whiskers [82], microbridges [48], and NWs [83]. Besides the ones we showed in Section 3, we add another interesting sample with pronouncing features, as shown in Fig. 4.3.

Such a Pb/ZnNW/Pb sample with a nanowire length of 60 μm was measured at 2 K with the magnetic field applied perpendicular to the wire. Compared to samples which only show steps at high magnetic fields, this sample has three steps in the dc *I-V* at zero field. Since the generation of phase-slip centers (PSC) contribute to the steps, this suggests that PSCs can exist even without an external disturbance if the sample itself has some intrinsic sources, *e.g*. structural defects. Apparently, this happens even when the sample has a zero resistance state. However, based on the *I-V* curve (black) in zero magnetic field, the transition at the first step already starts to become continuous (the bottom one in Fig. 3.4), compared to the one-step transition observed in other samples. This may suggest the start of the collapse of the superconducting state.

Another interesting feature we have observed in Fig. 4.3 is the random jumping between two continuous *I-V* parts separated by a single step. Besides suggesting the existence of a meta-stable state, this further suggests that the generation of one step corresponds to the addition of a resistive portion along the wire [48]. Such increase in resistance reduces the current and hence may bring the resistive state back to the superconducting zero-resistance state. The random jumping also suggests the stochastic nature of the generation of PSCs [37].

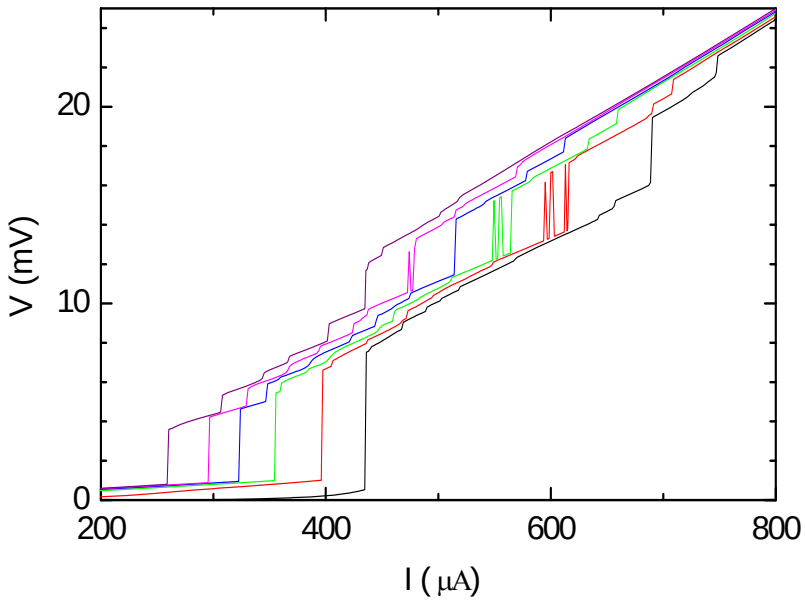

FIG. 4.3. *I-V* curves measured on a 60 μm Zn nanowires with Pb electrodes at 2.0 K in transverse fields. The fields are 1.0, 1.2, 1.4, 1.6, 1.8. and 2.0 kOe for curves from the right to the left

The random jumping feature was observed in a number of samples. The one shown in Fig. 4.4 displays more pronounced effects. Considering the jumping mechanism as described above, the number of jumps near one step should increase with smaller ramping rate of the current. Such experiments have been done for the sample in Fig. 4.4. Results were consistent with this prediction.

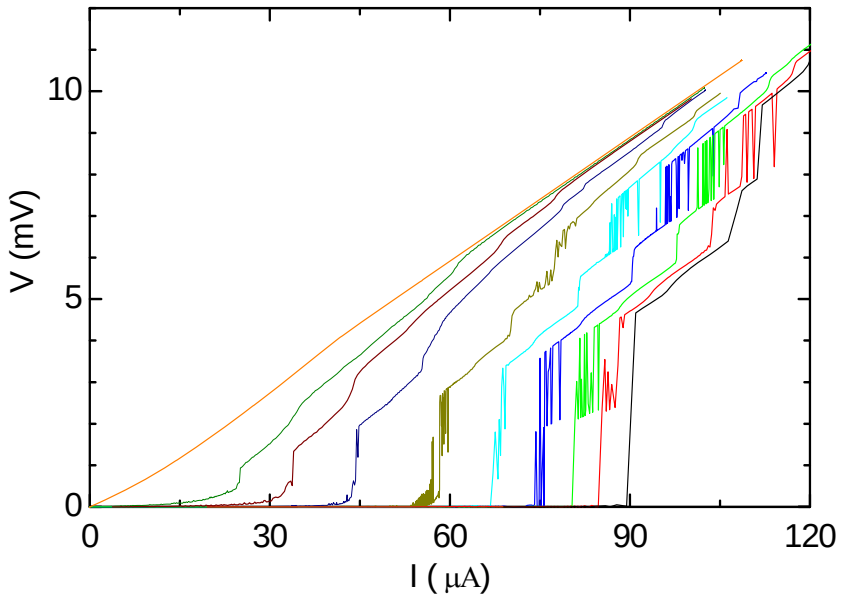

FIG. 4.4. *I-V* curves measured on a Zn nanowires with Sn electrodes in zero field. They were measured at temperatures of 3.70, 3.50 , 3.40 , 3.25, 2.75, 2.50, 2.25, and 1.80 Kelvin for curves from the left to the right

The observation of PSCs is not only useful for identifying the details in the collapsing of a superconducting condensate. More importantly, it gives useful information for understanding the long-range proximity effect. As a demonstration, current-biased *I-V* curves were measured on a Sn NW at 2 K for various transverse fields, and plotted in Fig. 4.5 (a) for *H* between 0.8-2.5 kOe.

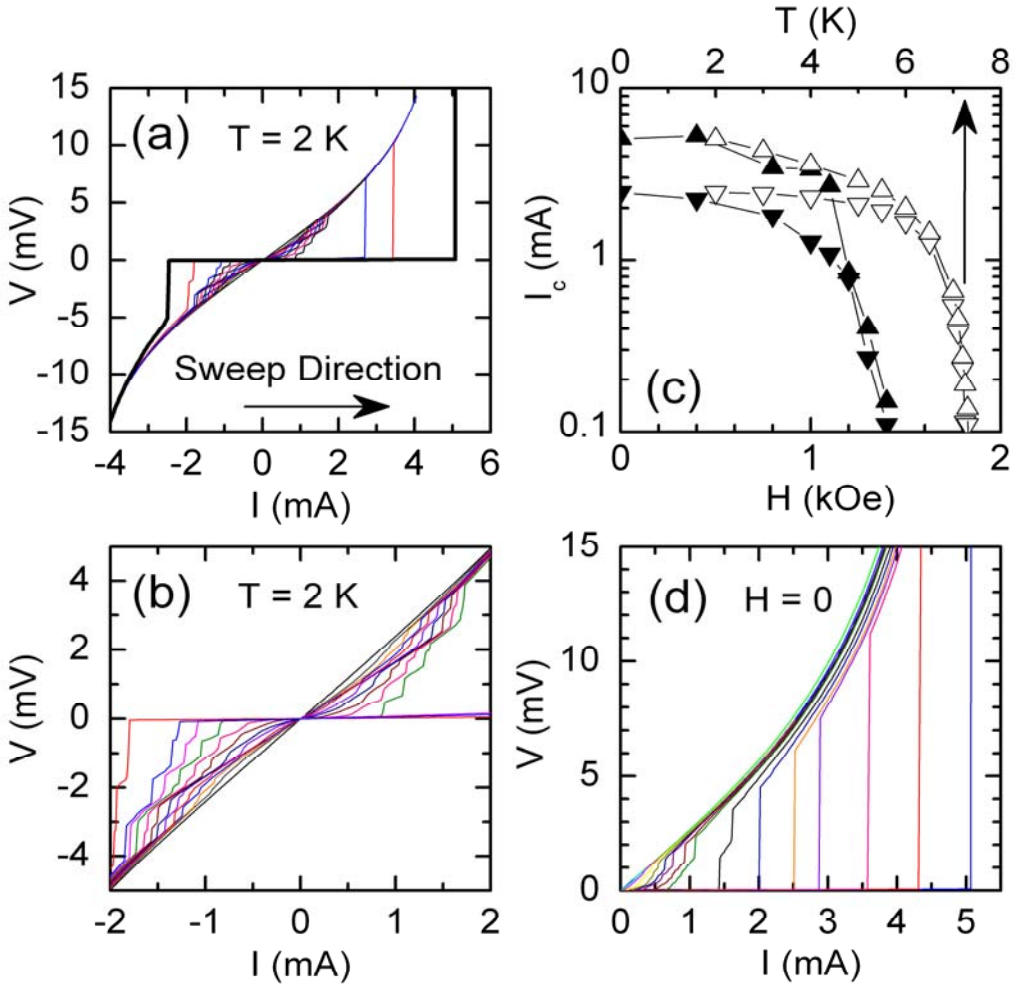

FIG 4.5. Dc *I-V* curves of a Pb/SnNW/Pb sample with changing temperature and magnetic field. (a): Hysteretic *I-V* curves measured at 2 K on a Sn NW with Pb electrodes for various transverse fields are shown for one sweep direction only for clarity. $H = 0$ for the thick black curve. I_c decreases with increasing H. (b): Data near the origin of (a) is re-plotted on a finer scale for H between 0.8 and 2.5 kOe to show the reproducible regular steps. (c) I_c vs. H (filled triangles) and I_c vs. T (open triangles) determined from the *I-V*s in (b) and (d). Up and down triangles are for the ascending and descending sides of the *I-V*s, respectively. (d) *I-V*s in zero field measured at $T = 2$, 3, 4, 5, 5.5, 6, 6.5, 7, 7.1, and 7.2 K for distinguishable curves from right to left

We identify the critical current I_c by the first step in an *I-V*, or, when the slope of an *I-V* shows a sudden increase from the slope at zero-bias for H very close to H_c. Fig. 4.5 (b) is a plot of I_c vs. H (filled triangles) at 2 K, showing that H_c is 1.3-1.4 kOe, consistent with H_c = 1.35 kOe obtained at 2 K in Fig. 4.5 (c).

The steps in the *I-V*s reveal the successive establishment of spatially localized phase-slip centers (PSCs) [48] as certain spots along a NW have smaller I_c. Associated with a PSC is an oscillating gap parameter [57] in a core length $2\xi(T)$, with $\xi \approx 230$ nm well below T_c for Sn [68]. The length of the PSCs is twice the non-equilibrium quasi-particles diffusion length Λ_Q [84]. Following Skocpol *et al.* [48], we found $2\Lambda_Q \approx 10$ μm using the voltage steps and the corresponding I_c, consistent with early results from Sn microbridges [48] and recent results from electroplated Sn NWs [60]. Similar multiple steps were also observed in *I-V*s measured between 6.5-7.2 K (near T_c(Pb)) in zero field, and we plot I_c vs. T in Fig. 4.5 (c) for $H = 0$ showing that $T_c = T_c$(Pb) as indicated by the arrow. Superconductivity was induced at T_c(Pb), as we did not observe any signature for a transition at T_c(Sn). We note that multiple steps were not observed in 6-μm-long NWs, possibly because this length was shorter than $2\Lambda_Q$.

The hysteretic *I-V* curves are shown again in Fig. 4.5, as we have seen in several examples in Section 3. This phenomenon has been previously observed in other systems [55, 75, 85]. The hysteresis is often characterized by the difference between the switching current I_s and the retrapping current I_r [37]. The switching current is the current level at which the measured sample switches from a zero voltage (or very low voltage) stage to a resistive state by increasing the bias current. The widely used

definition of the critical current, I_c, is often equivalent to I_s. Accordingly, the retrapping current is defined as the current value at which the measured sample switches back down to zero voltage with decreasing current. As found by both our own experiments and reports from others, I_r is quite accurately reproduced from sweep to sweep, since it reflects the minimum current level at which the Ohmic resistive state is stable. However, I_s can be different on each successive sweep, reflecting the stochastic nature of the fluctuation-induced switching process [37]. But it has a reasonably well-defined average value. This has been observed in our experiments. The stochastic nature is demonstrated by the random jumping of voltage between two steps shown in Fig. 4.4.

The hysteretic *I-V* curves was observed earlier in superconducting filaments and explained in terms of self-heating hotspots [86]. Recently, improved understanding of the hotspot model suggests its close relation to the understanding of the PSCs [37]. This is because the heating in the superconducting state is always related to the finite resistance generating by phase-slips and hence contributes to the generation of hotspots. Similar behavior was also observed in under-damped Josephson junctions [37], where the dissipative coupling to the environment in the tilted washboard potential of the Josephson junctions creates phase instability. The run-away and retrapping of the phase point, without regard to heating, produces such hysteresis. In recent reports of the proximity induced superconductivity in carbon nanotubes [87], semiconductor nanowires [88], and graphene [74], hysteresis has also been observed constantly. In these reports, the hysteretic phenomenon was either explained in terms of under-damped Josephson junction, or the hotspot model. In a recent theoretical work by Tinkham, *et al*

[89], by only considering the classical heating effects based on the measured $R(T)$ data instead of a microscopic model of phase slip rates, the authors were able to account for the hysteretic nature of the *I-V* curves.

To investigate the mechanism for the hysteresis in our nanowire samples, we have tried to measure the *I-V* curves with different sweeping rates, dwelling time between different sweeps, and staying different intervals at the highest current point. The typical data was shown in Fig. 3.6. If Joule heating is the major reason for such an effect, sweeps with different rates in the high current regime should show significantly different slope in dc *I-V* curves. However, such a difference was not observed. All the sweeps follow the same trace in the high current regime. Even after a prolonged stay at the same current spot, the slope was not changed. The bias current actually determined the slope and voltage value, excluding contribution from time related factors, on which the heating effect should be linearly depending. These results indicate that the hysteresis observed in superconducting nanowires is not, or at least, not fully generated by the Joule heating effect. This also can be further understood by considering the special geometry of the sample. A superconducting nanowire falls into the middle of the two cases described above. Phase-slip centers act qualitatively like weak link Josephson junctions in series. The heating effects can also be very important because of the difficulty in dissipating Joule heat through a long wire. For our samples, since the wires are thermally connected to the molecular membrane throughout the whole length, Joule heating may turn out to be a less important factor.

4.3 Proximity effect versus residual-resistance-ratio (RRR)

The anomalous proximity effect has been consistently observed in about 160 NWs with various electrodes. As we have already stated, the unique combination of the high quality of the wires and the contact transparency likely plays an important role in the observed proximity effect. In Section 2, the single crystal structure of the nanowires illustrated by TEM studies confirms the quality of the nanowires.

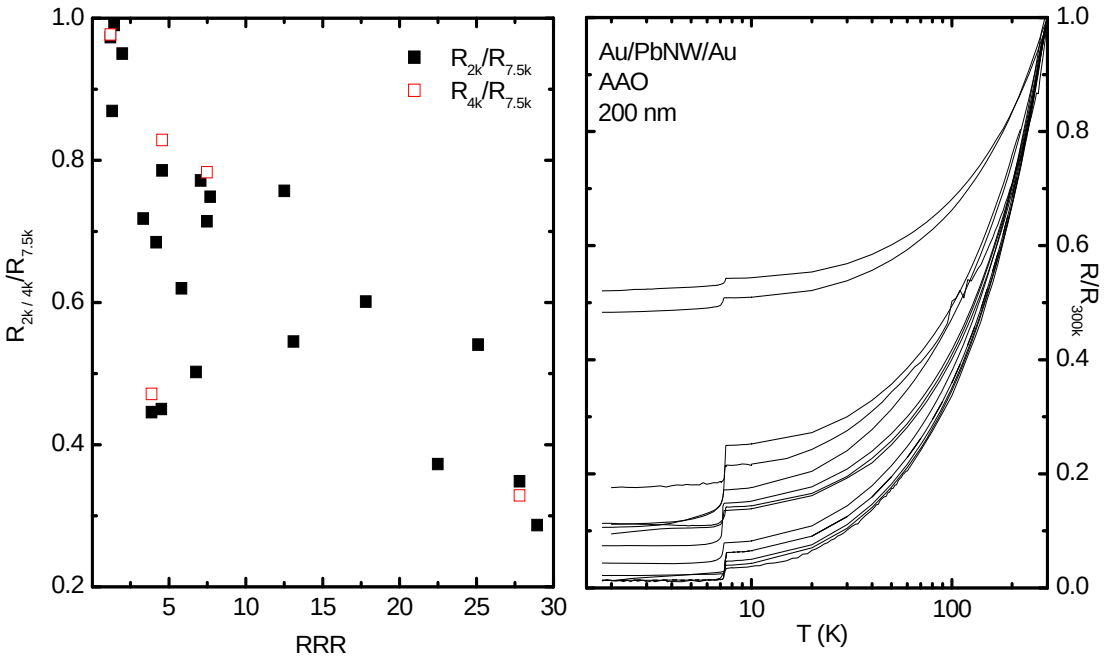

FIG. 4.6. Suppression of superconductivity in long Au/PbNW/Au samples versus RRR. Right: normalized R-T curves; Left: *R*(2K)/*R*(7.5K) or *R*(4K)/*R*(7.5K) versus RRR for each sample in the right graph

It is generally true that single-crystal wires make good conductors and hence elongate the superconducting coherence generated by the electrodes [90, 91]. In this subsection, I am going to use the residual-resistance-ratio (RRR) as a parameter that we obtain in transport measurements to further study the relation between the quality of the wires and the strength of the proximity effect.

For the *R*-*T* data shown in Fig. 3.2 for long Au/PbNW/Au samples, we plot again $R(T)/R(300\text{K})$ vs. the logarithm of T up to 300 K in Fig. 4.6. This log(T) graph gives both the R behavior in the full temperature range and the detailed structure at low temperatures. To characterize the proximity effect caused by the normal Au electrodes, we mornalize the non-zero resistance below T_c, $R(2\text{K})$ or $R(4\text{K})$ depending on which better represents the trend, by the resistance above the transition temperature, $R(7.5\text{K})$ to characterize the strength of the proximity effect. The RRR was easily calculated by using the inverse of $R(7.5\text{K})/R(300\text{K})$ obtained in the *R*-*T* curves. Although the dots don't converge to a straight line, a clear trend is obvious: samples with bigger RRR tend to be less resistive below T_c. In other words, wires with higher quality tend to have stronger superconducting state that is less affected by the normal electrodes connected to them.

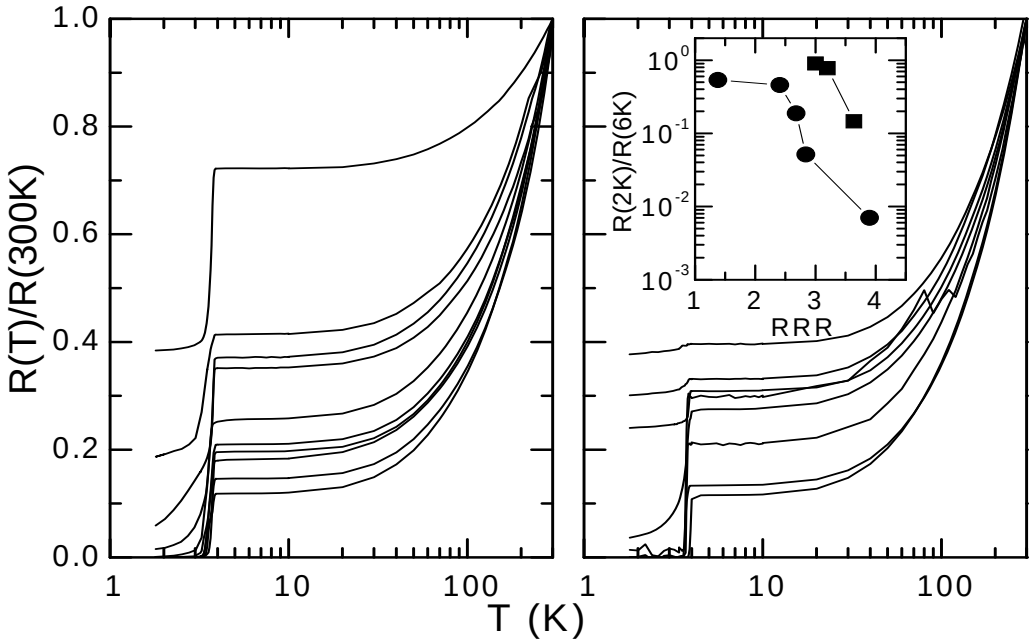

FIG. 4.7. Normalized *R*-*T* data of short (left) and long (right) Sn/ZnNW/Sn samples. Inset: *R*(2K)/*R*(6K) plotted against RRR of selected samples in the left graph

On the other hand, superconducting electrodes should have stronger effect on the normal nanowires connected between them. We use data obtained on Sn/ZnNW/Sn structures to illustrate this point. Data from both long (60μm) and short (6μm) wires are plotted in Fig. 4.7.

By using similar techniques we employed in Fig. 4.6, we plot in the inset of Fig. 4.7 R(2K)/R(6K) versus RRR for these sample. However, for many samples with practically zero resistance below the transition temperature, it is not meaningful to plot R(2K)/R(6K) versus the RRR values. Therefore, only the ones with finite resistance values below the transition temperature are shown in the inset of Fig. 4.7. The logarithm of R(2K)/R(6K) illustrates a certain trend in how the proximity effect depends on RRR.

In using the normalized resistance to characterize the proximity effect, we have observed that for samples with zero residual resistance, the rate of resistance drop below the transition temperature shows a systematic dependence on RRR. Therefore, we plot the slope of the resistance versus the temperature curve below the transition temperature as a function of RRR. Such analyses have been done systematically for both types of samples and the results are presented in Fig. 4.8. Graph (a) shows that induced superconductivity in NWs with small RRR was partial. Well bellow T_c(Sn), the residual resistance and the resistance tail decreased consistently with increasing RRR. In Fig. 4.8 (b), we plot for various samples the slope of the low-T resistance tail $d[ln(R(T))]/d[lnT]$ versus RRR, with open (filled) symbols for 6-μm-long (60-μm-long) NWs.

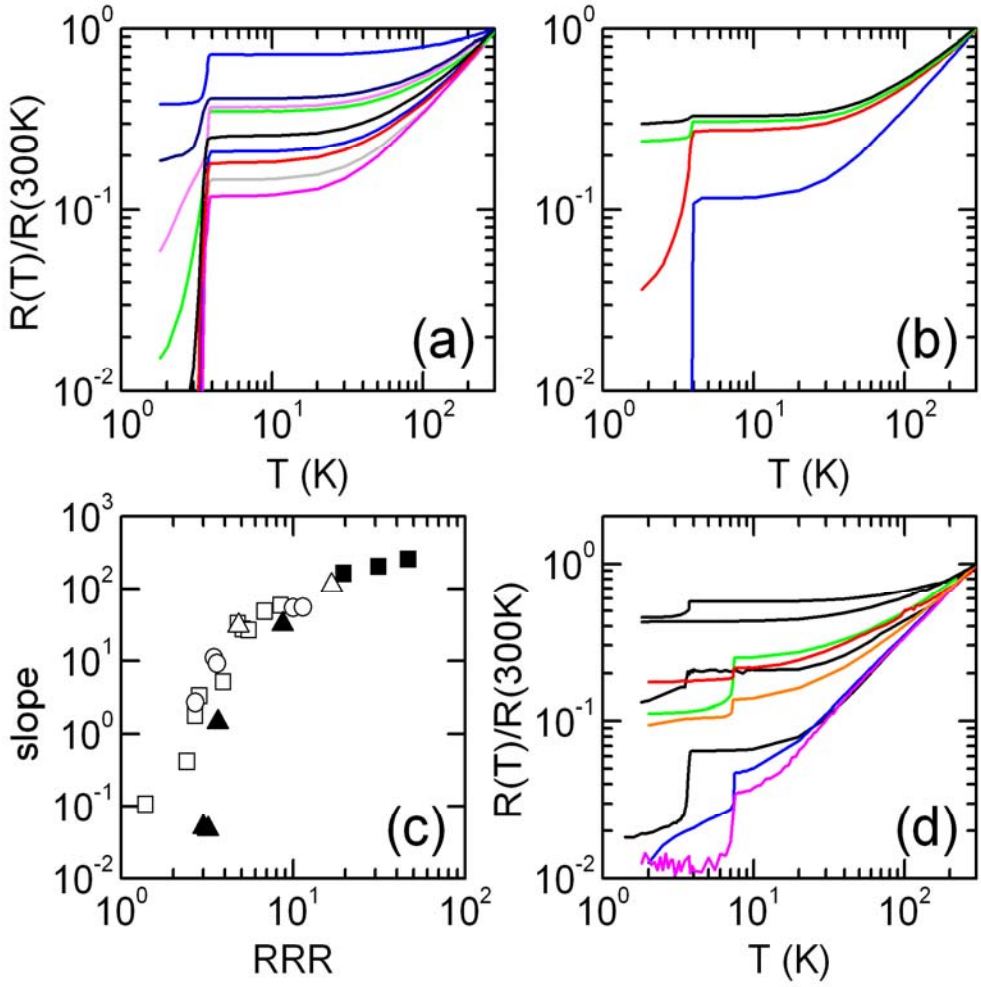

FIG. 4.8. Proximity effect and RRR in various samples. (a): Normalized *R* vs. *T* for 6-μm-long Zn NWs with Sn electrodes. Diameters were 30, 80, 80, 80, 30, 30, 80, and 50 nm for curves from the top to the bottom. (b): Normalized *R* vs. *T* for 60-μm-long Zn NWs of diameter 200 nm with Sn electrodes. (c): The slope of the low-*T* resistance tail vs. RRR for various samples. Open symbols are for 6-μm-long NWs: ○ for Sn NWs with Pb electrodes, □ for Zn NWs with Sn electrodes, and Δ for Zn NWs with Pb electrodes. Filled symbols are for 60-μm-long NWs: ▲ for Zn NWs with Sn electrodes and ■ for Sn NWs with Pb electrodes. (d): Normalized R vs. T for 60-μm-long Sn (black curves) and Pb (non-black curves) NWs with Au electrodes

For 6-μm-long NWs, partially induced superconductivity for RRR < 2 may still be explained by coherence over the length L_T, however, the sharp increase in $d[ln(R(T))]/d[lnT]$ for larger RRR values signals the onset of a new long-range PE. We also observe in the lower part of Fig. 4.8 (b) that, for NWs having small RRR values, induced superconductivity was much weaker in 60-μm-long NWs than in 6-μm-long NWs. The highest RRR values for our NWs of d = 200 nm was near 50. In comparison, earlier measurements of annealed bulk samples of Pb, Sn, and Zn obtained RRR of 25-33, 75-85, and 67-77, respectively. For the Sn NW (d = 200) in Fig. 4.8 (d), the residual resistance above T_c was ~ 5 Ω, giving a resistivity $\rho \sim 0.26$ μΩcm. Using the Drude model [77] and treating the system as a free-electron Fermi gas, we obtain an elastic mean-free-path $l = 3\pi^2/(e^2k_F^2\rho) = 180$ nm, where $k_F = 1.6\times10^8$ cm^{-1} is the Fermi wavevector and e is electron charge. We find that, for NWs having the largest RRR values in each diameter group, l appears to be limited by d: l = 180 nm for d = 200 nm; l = 35 nm for d = 30 nm; l = 55 nm for d = 60 nm; l = 70 nm for d = 80 nm. However, besides setting an upper limit on l, the role of the diameter in the observed PE is not clear. In this study, $d < \xi$ for Sn ($\xi \approx 230$ nm) and Zn ($\xi \approx 2$ μm) [68]. Studies of the crossover to $d > \xi$ are highly desirable.

5. CONCLUSIONS AND FUTURE WORK

5.1 Conclusions

In conclusion, an anomalous long-range superconducting proximity effect has been observed in an electrode-nanowire-electrode system. With electrodes having a higher critical temperature T_c, single-crystal Zn and Sn NWs of length up to 60 μm are superconducting at the T_c of the electrodes. The resistive transitions and I-V curves measured at various H and T further confirm this long-range PE. The value of RRR appears to play an important role.

We summarize below the data and analysis presented in Sections 3 and 4 to highlight what we have achieved so far:

1) We have successfully fabricated a series of electrode-nanowire-electrode devices to study the proximity effect in superconducting nanowires. Our experimental methods have achieved both high quality of the nanowires (single-crystal) and the nanowire-electrode contact.
2) Our transport studies of the fabricated structures have demonstrated a complete suppression of superconductivity by normal metal electrodes at the length scale of 6 μm and partial suppression at the length scale of 60 μm.
3) The proximity-induced superconductivity has been found to be robust in 60-μm-long Zn and Sn nanowires by electrodes with higher transition temperatures.

This length scale is much larger than any previously reported range of superconducting proximity effect.

4) Observation of regular steps in the dc *I-V* curves suggests the successive generation of phase-slip centers (PSC) along the nanowires. The phenomenon of PSC has been consistently observed in proximity-induced superconducting nanowires. Analyses of the size of the PSCs are helpful to further understanding the long-range proximity effect.

5) Hysteresis was observed in the dc *I-V*s of many long nanowires. We find that Joule heating can't explain the hysteresis. Joule heating is closely related to the generation of PSCs in the low resistance state.

6) Both sharp and smooth transitions near the critical current in the dc *I-V* curves have been observed in different samples as well as in a single sample but at various magnetic fields and temperatures. This provides further evidence for the interaction of superconductivity in nanowires with the environment and external disturbance. The multi-peak features in the ac *I-V*s manifest multiple Andreev reflections at the S-N interfaces existing along the nanowires.

7) A clear dependence of the proximity effect on the RRR values of the nanowire structure has been found. This observation offers clues for understanding the long-range proximity effect.

8) The microscopy studies we have carried out to investigate the compositional and structural details of the fabricated device form the most thorough investigation of nanowire related structures using template based electro-deposition method.

It has revealed the details on the structural and chemical composition of the samples, and provided strong support to the observed anomalous long-range superconducting proximity effect.

5.2 Future work

Future work in this project will be focused on confirmation and further investigation of the physical phenomena. The most applicable approach to confirm the effect is to carry out transport measurements and microscopy studies on the same nanowires. We are planning to combine lithography technique and etching to limit the area for nanowires to make electrical contact so that we can locate the exact wire we measure in transport studies. To further clarify the features in the *I-V* curves and the relation between RRR and the proximity effect, more experiments will be performed with samples having a broad range of RRR values.

Below is a summary of possible future work that can be done to further understand the proximity effect.

1) We can measure short Au/PbNW/Au or Au/SnNW/Au samples, where superconductivity is fully suppressed, to even lower temperature range by using a dilution refrigerator. Signatures of superconductivity may occur due to stronger pairing potential at lower temperature.
2) More studies can be carried out to systematically control nanowire growth conditions to produce samples having desirable RRR values. In such way, we can study long Pb/SnNW/Pb samples with partial induction of superconductivity

due to small RRR. Resistance of such samples should have further drops around near the Sn transition temperature.

3) For long Pb/ZnNW/Pb samples with small RRR, finite resistance was found below the Pb transition temperature. Experiments measuring the resistance of the device near the Zn bulk transition temperature would be interesting. Such experiments have to be done using a dilution refrigerator.

4) It will be ideal if we can image and measure the same nanowire. Efforts in combing electro-deposition and lithography techniques are worthwhile in this regard while still using the molecular membrane as templates. The self-contacting method should be used to maintain good contact quality.

5) We can also use the traditional e-beam lithography to define superconducting leads on electroplated single-crystal nanowires. However, as we stated earlier, special treatment has to be done to improve the contact transparency.

One may question the effect of superconducting electrodes if the NWs are made of normal metals or materials having a higher critical temperature. Our experiments did not test these possibilities since we have not found proper materials to fabricate such samples. With the *in situ* method, we can only plate NW materials having a higher reactivity than that of the electrode materials.

REFERENCES

[1] C. A. Huber *et al.*, Science **263**, 800 (1994).

[2] C. R. Martin, Science **266**, 1961 (1994).

[3] R. F. Service, Science **295**, 946 (2002).

[4] M. S. Gudiksen *et al.*, Nature **415**, 617 (2002).

[5] K. Lin *et al.*, J Vac Sci Technol B **9**, 3511 (1991).

[6] Y. K. Kwong *et al.*, Phys Rev B **45**, 9850 (1992).

[7] T. Thurn-Albrecht *et al.*, Science **290**, 2126 (2000).

[8] K. Yoshino *et al.*, Fullerene Science and Technology **7**, 695 (1999).

[9] V. V. Pokropivny, Physica C-Superconductivity and Its Applications **351**, 71 (2001).

[10] S. Hoeppener *et al.*, Adv Mater **14**, 1036 (2002).

[11] Z. L. Wang, and J. H. Song, Science **312**, 242 (2006).

[12] L. J. Lauhon *et al.*, Nature **420**, 57 (2002).

[13] W. Schwarzacher *et al.*, J Magn Magn Mater **199**, 185 (1999).

[14] N. A. Melosh *et al.*, Science **300**, 112 (2003).

[15] S. Valizadeh *et al.*, Adv Funct Mater **12**, 766 (2002).

[16] M. L. Tian *et al.*, Nano Lett **3**, 919 (2003).

[17] D. M. Davis, and E. J. Podlaha, Electrochem Solid St **8**, D1 (2005).

[18] M. C. Kum *et al.*, Nanotechnology **19**, 325771(2008).

[19] M. L. Tian *et al.*, Nano Lett **5**, 697 (2005).

[20] H. Masuda *et al.*, Adv Mater **13**, 189 (2001).

[21] S. Shingubara *et al.*, J Vac Sci Technol B **19**, 1901 (2001).

[22] S. Shingubara *et al.*, Jpn J Appl Phys 1 **36**, 7791 (1997).

[23] J. G. Wang *et al.*, J Phys Chem B **108**, 841 (2004).

[24] J. Joo *et al.*, Nanotechnology **17**, 3506 (2006).

[25] Z. H. Zhong *et al.*, Science **302**, 1377 (2003).

[26] Y. Nakayama *et al.*, Nature **447**, 1098 (2007).

[27] T. Ohgai *et al.*, J Phys D Appl Phys **36**, 3109 (2003).

[28] Y. T. Pang *et al.*, J Phys-Condens Mat **14**, 11729 (2002).

[29] M. L. Tian *et al.*, Appl Phys Lett **83**, 1620 (2003).

[30] M. L. Tian *et al.*, Phys Rev B **71**, 104521(2005).

[31] S. Michotte *et al.*, Appl Phys Lett **85**, 3175 (2004).

[32] G. Yi, and W. Schwarzacher, Appl Phys Lett **74**, 1746 (1999).

[33] X. Y. Zhang, and J. Y. Dai, Nanotechnology **15**, 1166 (2004).

[34] A. Bezryadin, C. N. Lau, and M. Tinkham, Nature **404**, 971 (2000).

[35] P.-G. d. Gennes, *Superconductivity of Metals and Alloys* (Advanced Book Program, Perseus Books, Reading, MA, 1999).

[36] R. D. Parks, *Superconductivity* (M. Dekker, New York, 1969).

[37] M. Tinkham, *Introduction to superconductivity* (McGraw Hill, New York, 1996).

[38] S. Michotte, S. Matefi-Tempfli, and L. Piraux, Appl Phys Lett **82**, 4119 (2003).

[39] D. Y. Vodolazov *et al.*, Phys Rev Lett **91,** 157001 (2003).

[40] H. Kraus, Jpn J Appl Phys 1 **37**, 6273 (1998).

[41] N. Bluzer, and M. G. Forrester, Opt Eng **33**, 697 (1994).

[42] C. N. Lau *et al.*, Phys Rev Lett **87,** 217003 (2001).

[43] J. E. Mooij, and Y. V. Nazarov, Nat Phys **2**, 169 (2006).

[44] M. Tinkham, and C. N. Lau, Appl Phys Lett **80**, 2946 (2002).

[45] M. Zgirski *et al.*, Nano Lett **5**, 1029 (2005).

[46] A. Rogachev *et al.*, Phys Rev Lett **97,** 137001 (2006).

[47] M. Tian *et al.*, Phys Rev Lett **95,** 076802 (2005).

[48] W. J. Skocpol, M. R. Beasley, and M. Tinkham, J Low Temp Phys **16**, 145 (1974).

[49] J. Meyer, and G. Minniger., Phys Lett A **38**, 529 (1972).

[50] J. P. Maneval *et al.*, J Supercond **14**, 347 (2001).

[51] J. P. Maneval *et al.*, J Supercond **15**, 417 (2002).

[52] H. Courtois, P. Gandit, and B. Pannetier, Phys Rev B **52**, 1162 (1995).

[53] J. A. van Dam *et al.*, Nature **442**, 667 (2006).

[54] P. Jarillo-Herrero, J. A. van Dam, and L. P. Kouwenhoven, Nature **439**, 953 (2006).

[55] A. Y. Kasumov *et al.*, Science **284**, 1508 (1999).

[56] T. M. Klapwijk, J Supercond **17**, 593 (2004).

[57] G. E. Blonder, M. Tinkham, and T. M. Klapwijk, Phys Rev B **25**, 4515 (1982).

[58] F. Zhou, B. Spivak, and A. Zyuzin, Phys Rev B **52**, 4467 (1995).

[59] C. C. Chi *et al.*, Phys Rev B **50**, 3487 (1994).

[60] D. Lucot *et al.*, Appl Phys Lett **91,** 042502 (2007).

[61] H. D. Liu *et al.*, Physica C **468**, 304 (2008).

[62] W. H. Wu *et al.*, Appl Phys Lett **84**, 966 (2004).

[63] H. Pan *et al.*, Nanotechnology **16**, 1559 (2005).

[64] S. Michotte *et al.*, Physica C **377**, 267 (2002).

[65] L. Piraux *et al.*, J Nanosci Nanotechno **5**, 372 (2005).

[66] H. Masuda *et al.*, Appl Phys Lett **71**, 2770 (1997).

[67] H. Schwanbeck, and U. Schmidt, Electrochim Acta **45**, 4389 (2000).

[68] C. Kittel, and P. McEuen, *Introduction to Solid State Physics* (J. Wiley, Hoboken, NJ, 2005).

[69] G. R. Boogaard *et al.*, Phys Rev B **69** (2004).

[70] S. Michotte, S. Matefi-Tempfli, and L. Piraux, Supercond Sci Tech **16**, 557 (2003).

[71] Z. X. Ye *et al.*, Physica B **403**, 1529 (2008).

[72] H. I. Jorgensen *et al.*, Phys Rev Lett **96,** 026403 (2006).

[73] J. Jiang *et al.*, Phys Rev B **68** (2003).

[74] H. B. Heersche *et al.*, Nature **446**, 56 (2007).

[75] Y. J. Doh *et al.*, Science **309**, 272 (2005).

[76] J. P. Cleuziou *et al.*, Nature Nanotechnology **1**, 53 (2006).

[77] N. W. Ashcroft, and N. D. Mermin, *Solid State Physics* (Holt, Rinehart and Winston, New York, 1976).

[78] G. Slama, and R. Tidecks, Solid State Commun **44**, 425 (1982).

[79] H. Courtois *et al.*, Phys Rev Lett **76**, 130 (1996).

[80] H. D. Liu *et al.*, Physica B **403**, 1542 (2008).

[81] R. J. Fitzgerald, S. L. Pohlen, and M. Tinkham, Phys Rev B **57**, R11073 (1998).

[82] R. Tidecks, and G. Slama, Z Phys B Con Mat **37**, 103 (1980).

[83] S. Michotte *et al.*, Phys Rev B **69,** 094512 (2004).

[84] M. Octavio *et al.*, Phys Rev B **27**, 6739 (1983).

[85] A. Kasumov *et al.*, Phys Rev B **68,** 214521 (2003).

[86] W. J. Skocpol, M. R. Beasley, and M. Tinkham, B Am Phys Soc **18**, 302 (1973).

[87] R. Lopez, M. S. Choi, and R. Aguado, Phys Rev B **75,** 045132 (2007).

[88] J. Xiang *et al.*, Nature Nanotechnology **1**, 208 (2006).

[89] M. Tinkham *et al.*, Physical Review B **68**, 134515 (2003).

[90] H. Courtois, P. Gandit, and B. Pannetier, Phys Rev B **51**, 9360 (1995).

[91] S. Gueron *et al.*, Phys Rev Lett **77**, 3025 (1996).

VITA

Haidong Liu received his Bachelor of Science degree in physics in 1999 from Jilin University, China. In August 1999, he entered the Department of Physics and started his research career as a research assistant in the Magnetic Materials Group of the National Laboratory of Solid State Microstructures at Nanjing University, where he received his Master of Science degree in condensed matter physics in July 2002. In the summer of 2002, he joined the Department of Physics at Texas A&M University as a graduate student. His research interests include the fabrication and characterization of metallic and semiconductor nanowires and nanotubes, the superconducting proximity effect in nanowires, electron transport properties of nanowires in general, and scanning probe microscopy. He received a Master of Science degree from Texas A&M University in the Materials Science and Engineering Program in May 2005.

Mr. Liu can be reached at haidongliu09@gmail.com. Direct mail can be addressed to: Department of Physics, TAMU 4242, Texas A&M University, College Station, Texas 77843-4242.